Proteomic Portraits Reveal Evolutionarily Conserved and Divergent Responses to Spinal Cord Injury

Authors

Michael A. Skinnider, Jason Rogalski, Seth Tigchelaar, Neda Manouchehri, Anna Prudova, Angela M. Jackson, Karina Nielsen, Jaihyun Jeong, Shalini Chaudhary, Katelyn Shortt, Ylonna Gallagher-Kurtzke, Kitty So, Allan Fong, Rishab Gupta, Elena B. Okon, Michael A. Rizzuto, Kevin Dong, Femke Streijger, Lise Belanger, Leanna Ritchie, Angela Tsang, Sean Christie, Jean-Marc Mac-Thiong, Christopher Bailey, Tamir Ailon, Raphaele Charest-Morin, Nicolas Dea, Jefferson R. Wilson, Sanjay Dhall, Scott Paquette, John Street, Charles G. Fisher, Marcel F. Dvorak, Casey Shannon, Christoph Borchers, Robert Balshaw, Leonard J. Foster, and Brian K. Kwon

Correspondence

foster@msl.ubc.ca; brian.kwon@ubc.ca

In Brief

Kwon, Foster, and colleagues perform targeted proteomic analysis of serially collected CSF and serum samples from 111 patients with acute spinal cord injury. The same proteomic methods were applied in parallel to an experimental study of SCI in a large animal model. The authors characterize the molecular response to SCI in human patients, identify biomarkers of injury severity and recovery, and dissect the evolutionary conservation of the response to SCI across species.

Graphical Abstract

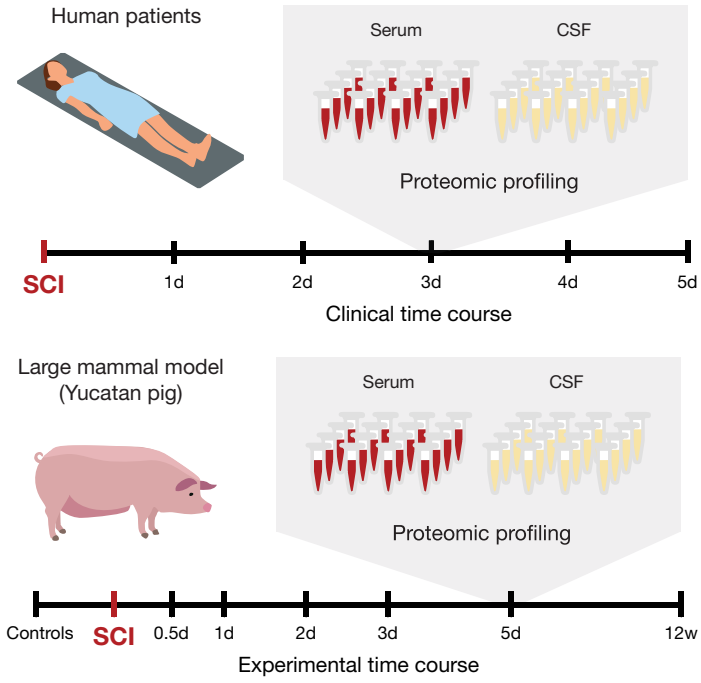

Highlights

- Targeted proteomic analysis of CSF and serum samples from 111 acute SCI patients.
- Single- and multiprotein biomarkers of injury severity and recovery.
- Parallel proteomic analysis in a large animal model identifies conserved biomarkers.
- Evolutionary conservation and divergence of the proteomic response to SCI.

2021, Mol Cell Proteomics *20*, 100096

https://doi.org/10.1016/j.mcpro.2021.100096

Proteomic Portraits Reveal Evolutionarily Conserved and Divergent Responses to Spinal Cord Injury

Michael A. Skinnider[1], Jason Rogalski[1], Seth Tigchelaar[2], Neda Manouchehri[2], Anna Prudova[1], Angela M. Jackson[3], Karina Nielsen[1], Jaihyun Jeong[1], Shalini Chaudhary[1], Katelyn Shortt[2], Ylonna Gallagher-Kurtzke[1,2], Kitty So[2], Allan Fong[2], Rishab Gupta[2], Elena B. Okon[2], Michael A. Rizzuto[2], Kevin Dong[2], Femke Streijger[2], Lise Belanger[4], Leanna Ritchie[4], Angela Tsang[4], Sean Christie[5], Jean-Marc Mac-Thiong[6,7], Christopher Bailey[8], Tamir Ailon[9], Raphaele Charest-Morin[10], Nicolas Dea[9], Jefferson R. Wilson[11], Sanjay Dhall[12], Scott Paquette[9], John Street[10], Charles G. Fisher[10], Marcel F. Dvorak[2,10], Casey Shannon[13], Christoph Borchers[3], Robert Balshaw[13], Leonard J. Foster[1,14,*], and Brian K. Kwon[2,10,*]

Despite the emergence of promising therapeutic approaches in preclinical studies, the failure of large-scale clinical trials leaves clinicians without effective treatments for acute spinal cord injury (SCI). These trials are hindered by their reliance on detailed neurological examinations to establish outcomes, which inflate the time and resources required for completion. Moreover, therapeutic development takes place in animal models whose relevance to human injury remains unclear. Here, we address these challenges through targeted proteomic analyses of cerebrospinal fluid and serum samples from 111 patients with acute SCI and, in parallel, a large animal (porcine) model of SCI. We develop protein biomarkers of injury severity and recovery, including a prognostic model of neurological improvement at 6 months with an area under the receiver operating characteristic curve of 0.91, and validate these in an independent cohort. Through cross-species proteomic analyses, we dissect evolutionarily conserved and divergent aspects of the SCI response and establish the cerebrospinal fluid abundance of glial fibrillary acidic protein as a biochemical outcome measure in both humans and pigs. Our work opens up new avenues to catalyze translation by facilitating the evaluation of novel SCI therapies, while also providing a resource from which to direct future preclinical efforts.

Each year, tens of thousands of individuals suffer an acute traumatic spinal cord injury (SCI) (1). The impact of the resulting neurological impairment on the physical, social, and vocational well-being of these individuals is profound (2). The burden on health care systems is likewise enormous (3). Decades of research in this field have generated numerous therapeutic interventions that have shown promise in preclinical studies (4, 5). However, among the handful that have emerged from the laboratory to be tested in the clinic, none have succeeded in demonstrating convincing neurological benefit.

In SCI, the primary traumatic insult to the spinal cord initiates a progressive cascade of secondary injury mechanisms, characterized by ischemia, excitotoxicity, apoptosis, demyelination, inflammatory cell infiltration and cytokine release, and the formation of a glial scar (6). Therapeutic approaches generally seek to curtail these responses, in order to improve neurological outcomes *via* neuroprotection. Interrogation of

From the [1]Michael Smith Laboratories and [2]International Collaboration on Repair Discoveries (ICORD), University of British Columbia, Vancouver, British Columbia, Canada; [3]UVic-Genome BC Proteomics Centre, Victoria, British Columbia, Canada; [4]Vancouver Spine Program, Vancouver, British Columbia, Canada; [5]Division of Neurosurgery, Dalhousie University, Halifax, Nova Scotia, Canada; [6]Department of Surgery, Hôpital du Sacrè-Coeur de Montrèal, Montrèal, Quebec, Canada; [7]Chu Sainte-Justine, Department of Surgery, Universitè de Montrèal, Montrèal, Quebec, Canada; [8]Division of Orthopaedic Surgery, London Health Sciences Centre, University of Western Ontario, London, Ontario, Canada; [9]Division of Neurosurgery and [10]Department of Orthopaedics, Division of Spine, University of British Columbia, Vancouver, British Columbia, Canada; [11]Division of Neurosurgery, University of Toronto, St Michael's Hospital, Toronto, Ontario, Canada; [12]Department of Neurosurgery, University of California San Francisco, San Francisco, California, USA; [13]Prevention of Organ Failure (PROOF) Centre of Excellence, Vancouver, British Columbia, Canada; and [14]Department of Biochemistry and Molecular Biology, University of British Columbia, Vancouver, British Columbia, Canada

*For correspondence: Leonard J. Foster, foster@msl.ubc.ca; Brian K. Kwon, brian.kwon@ubc.ca.

https://doi.org/10.1016/j.mcpro.2021.100096

these processes in human patients is limited by the inaccessibility of spinal cord tissue, and consequently, efforts to unravel this cascade rely almost entirely on animal models (7). The underlying assumption is that the pathological responses targeted in the animal setting will be similarly modulated in the injured human spinal cord. However, the failure of efforts to translate promising treatments from animal models into the clinic raises the possibility that important biological differences exist. As such, the dearth of data describing the pathobiology of SCI in human patients represents an obstacle to the development of new therapeutic approaches.

Once a promising intervention for SCI has emerged from the laboratory, the process of establishing efficacy in human patients is exceedingly challenging. Only a handful of large-scale clinical trials in acute SCI have ever been completed, each of which has highlighted the time and tremendous resources necessary for completion (8); more recent trials have experienced significant challenges in recruitment, leading to their premature termination. At the heart of this difficulty is the singular reliance on standardized neurological assessments for patient enrollment and evaluation of efficacy. These detailed examinations are challenging or impossible to perform in a substantial fraction of acutely injured patients, owing to concomitant trauma, intoxication, or sedation (9). Without a baseline evaluation, such individuals are rendered ineligible for clinical trials, severely limiting the pool of recruitable patients. Further compounding this challenge is the considerable variability in spontaneous recovery, even among patients classified similarly by the initial examination, which forces investigators to enroll large numbers of patients in order to discern treatment effects (10). With many promising new treatments vying for translation, the inability to validate them clinically presents a bottleneck to the progression of potentially effective therapies.

Clearly, for the field to move forward, new approaches are needed in the evaluation of novel therapeutics. Objective neurochemical biomarkers could catalyze a fundamental shift in the design and conduct of clinical trials for acute SCI (11). Diagnostic biomarkers of injury severity could facilitate the enrollment of acutely injured patients unable to complete a detailed neurological examination. Prognostic biomarkers of spontaneous neurological recovery could arguably have even greater utility, by reducing the number of patients needed to adequately power clinical trials. Markers that are similarly modulated in animal models, where outcome measures currently used to assess therapeutic efficacy lack a direct correlate in human, could provide a basis to prioritize therapies for translation into human trials (12). Finally, beyond advancing the development and translation of new therapies, biochemical tools capable of accurate prognostication also have obvious potential to guide acute and rehabilitative clinical management. However, previous efforts to identify biomarkers in acute SCI have been limited by small patient cohorts, few analytes measured, and lack of validation in an independent cohort (13–17).

Here, we describe a targeted proteomic analysis of cerebrospinal fluid (CSF) and serum samples serially collected over the first 5 days following acute SCI in a population of 111 patients. In parallel, we characterized CSF and serum samples from a porcine model of SCI, using an identical proteomic approach. In the patient population, we mine this resource to develop single- and multiprotein biomarkers of baseline injury severity and neurological recovery at 6 months post injury, and validate these in an independent cohort, demonstrating highly accurate patient stratification and prognostication. Through comparative proteomic analyses, we establish both conserved biological outcomes and species-specific responses between human SCI and a large animal model, including the discovery of glial fibrillary acidic protein (GFAP) as a cross-species outcome measure. With a total of 1329 samples analyzed, this biobank defines an unprecedented opportunity to interrogate the biology of acute traumatic SCI.

EXPERIMENTAL PROCEDURES

Experimental Design and Statistical Rationale

We performed parallel targeted proteomic analyses of serially collected CSF and serum samples from a prospective observational clinical trial (n = 111 patients with acute traumatic SCI and 21 uninjured controls) and an experimental study of SCI in a porcine model (n = 43 pigs). The objectives of the study were (1) to describe the acute pathophysiological responses to traumatic SCI over the early postinjury period in human patients; (2) to establish protein biomarkers for injury stratification and prognostication of neurological outcome; and (3) to establish both conserved biological outcome measures and species-specific responses between human SCI and a large animal model. The primary endpoints in the human clinical trial included baseline American Spinal Injury Association (ASIA) Impairment Scale (AIS) grade, change in total motor score (TMS) at 6 months post injury, and AIS grade improvement at 6 months post injury. Secondary endpoints, specified after initiation of the data analyses, included a baseline AIS grade of A, a change in TMS of seven or more points, and motor complete injury after 6 months. The primary endpoints in the pig study were baseline injury severity, as defined by the impactor height; hindlimb neurological recovery, as quantified on the Porcine Thoracic Injury Behavior Scale (PTIBS); and white matter tissue sparing, assessed histologically at 12 weeks post injury. Proteins whose abundance in the CSF or serum was associated with the primary endpoints were identified using linear models with empirical Bayes shrinkage as implemented in the R package “limma” (18). Multiprotein diagnostic and prognostic biomarkers of primary and secondary endpoints were developed using the python package “scikit-learn” (19). A total of 491 proteins were analyzed by parallel reaction monitoring (PRM)-MS in the CSF and multiple reaction monitoring (MRM)-MS in the serum. The clinical population comprised a discovery cohort of 91 patients and a successively enrolled validation cohort of 20 patients. Samples from the validation cohort were processed independently, and investigators were blinded to these data until the finalization of all statistical analyses in the discovery cohort.

Clinical Trial Enrollment

Individuals sustaining an acute SCI were enrolled into this prospective observational study (clinicaltrials.gov: NCT01279811) at four North American sites if they met the following inclusion criteria: (1) AIS grade A, B, or C on presentation; (2) spinal injury between C1 and L1; and (3) the ability to provide a valid, reliable neurological examination within 24 h of injury. Patients were excluded if they had concomitant brain injuries or concomitant major trauma to the chest, pelvis, or extremities that required invasive intervention (*e.g.*, chest tube, internal or external fixation) or were too sedated or intoxicated to provide a valid neurological examination. The uninjured control group consisted of 21 adult subjects undergoing routine lumbar decompressions and/or fusions who had no current or past history of SCI or myelopathy. The study was approved by the UBC Clinical Research Ethics Board (CREB; #H10-01091 for the clinical trial, #H08-00118 for normal controls) and conformed to the Declaration of Helsinki principles. Written informed consent to participate in the research was obtained from all patients.

Neurological Evaluation

The severity of neurological impairment was graded according to the standards of the International Standards for Neurological Classification of SCI examination, with motor scores recorded separately in the upper and lower extremities. All baseline testing and the assigning of the baseline AIS grade (A, B, or C) was conducted by research study nurses to confirm the initial examination of the patients. The baseline AIS grade was A for 73 patients, B for 19, and C for a further 19, where AIS A denotes complete motor and sensory paralysis, AIS B denotes complete motor paralysis but some preserved sensation, and AIS C is assigned when there is some preserved motor and sensory function. The International Standards for Neurological Classification of SCI examination was conducted again at 6 months post injury in all but one patient, who was lost to follow-up and excluded from analyses of neurological recovery, to determine whether the AIS grade had improved and the extent of TMS improvement.

Porcine Model

Female Yucatan miniature pigs (*Sus scrofa*) (Sinclair Bio-resources), aged approximately 150 to 200 days and weighing 20 to 30 kg, were group housed at a large animal facility for 5 weeks prior to surgery. Animals were block randomized into different injury severity groups or a sham group. Animals in the sham group received an identical laminectomy surgery as in the injured groups but no weight drop injury or compression to the spinal cord. Three different injury severities were induced by dropping a 50 g weight onto the exposed spinal cord from a height of 40, 20, or 10 cm, followed by 5 min of compression with a 150 g weight. Surgical procedures for experimental SCI and postoperative care were as described (20, 21). Briefly, using anatomical landmarks, the T9, T10, and T11 pedicles were cannulated and instrumented with screws (SelectTM Multi Axial Screw). After the T10 laminectomy was performed, the weight drop device was rigidly secured to the pedicle screws and positioned so that the impactor would fall directly on the exposed dura and spinal cord at T10. All animal experiments were approved by the University of British Columbia Animal Care Committee (#A16-0311) and conducted in strict adherence to the guidelines issued by the Canadian Council for Animal Care.

Porcine Neurological Evaluation

The PTIBS was used to assess hindlimb functional recovery, as described (20). Briefly, 4 weeks prior to injury, animals were trained to walk straight at a constant speed without stopping. Baseline behavior was obtained for each animal, 1 week prior to surgery; five runs were recorded using three high-definition camcorders placed 30 cm above the ground and behind the animals. Functional assessment resumed 1 week post injury and continued once weekly for 12 weeks. The functional assessment footage was analyzed by two independent observers who were blinded to the biomechanical severity of spinal cord injury that was induced at the time of surgery. The PTIBS scale ranges from no active hindlimb movements (score 1) to normal ambulation (score 10). PTIBS scores of 1 to 3 are characterized by "hindlimb dragging," scores of 4 to 6 reflect varying degrees of "stepping" ability, and scores of 7 to 10 reflect varying degrees of "walking" ability.

Porcine Histological Evaluation

Tissue sparing was assessed by histological analysis at the end of the experiment (12 weeks post injury), at which point animals were euthanized by sodium pentobarbital (120 mg/kg) and the spinal cord was harvested, postfixed, and cryoprotected as described (22). Subsequently, spinal cords were cut into 1-cm blocks centered on the site of injury, frozen on dry ice, and stored at –80 °C. Cross-sections (20-μm thick) were then cut using a cryostat. Sections were serially mounted onto adjacent silane-coated SuperFrost Plus slides (Fisher Scientific) and stored at –80 °C. For differentiating gray and white matter, Eriochrome Cyanine R staining was performed with Neutral Red as a counterstain. The Eriochrome Cyanine R–stained sections were examined and micrographs (5× objective, Zeiss AxioImager M2 microscope) were taken of sections at 800-μm intervals throughout the lesion site. The spinal cord outer perimeter, white matter, and gray matter were outlined, and the area of each was calculated using Zen Imaging Software (Carl Zeiss Canada Ltd). The percentages of white matter and gray matter were calculated by dividing the spared white or gray matter by the total area of the spinal cord on a given section, with the sum of the two representing spared tissue.

Sample Collection

Collection of CSF samples from enrolled patients was achieved using an intrathecal catheter (Braun Medical Inc) inserted before the surgical procedure in the lumbar spine at L2/3 or L3/4 using a standard aseptic technique. The catheter was advanced 15 to 20 cm from the entry point on the skin surface and kept in place for 5 days. Samples of 3 to 4 ml were drawn at the time of catheter insertion and then in the subsequent postoperative period, approximately three times per day, discarding the first 1 ml of CSF aspirated. For the non-SCI control group, samples were acquired during the operation after the lumbar spine had been exposed. Sample processing was performed immediately at the patient's bedside by the research study nursing team. CSF samples were centrifuged at 1000*g* for 10 min. Blood samples were incubated at room temperature for 25 min, then centrifuged at 10,000*g* for 5 min. CSF and serum supernatants were collected and dispersed into 200-μL aliquots, then immediately frozen in an ethanol-dry ice bath and stored at -80 °C.

Serial collection of porcine samples was performed 15 min prior to injury, and then again at 12 h, 24 h, 48 h, 72 h, 120 h, and 12 weeks post injury, as described (21, 23). Briefly, CSF collection was achieved using a 19-gauge epidural catheter (Braun Medical Inc) inserted into the intrathecal space with the catheter tip resting approximately 8 cm caudal to the injury site. A total of 1 ml of CSF was collected and immediately centrifuged at 1000*g* for 10 min at room temperature. Serum collection was performed by inserting an 8F Groshong catheter (Bard Access Systems) in the left external jugular vein. This was connected to a low-volume titanium subcutaneous access port (X-port; Bard Access Systems) housed in the posterior neck region. A total of 5 ml of whole blood was collected. To separate the serum portion, blood was allowed to incubate for 25 min at room temperature and then centrifuged at 10,000*g* for 5 min.

Targeted Proteomic Assays

Serum protein quantitation was achieved using an expanded and updated version of a previously described MRM panel (24, 25) targeting 270 proteins. These peptides had been previously validated for their use in LC-MRM experiments following the Clinical Proteomic Tumor Analysis Consortium guidelines for assay development (Clinical Proteomic Tumor Analysis Consortium Assay Characterization Guidance Documents. https://proteomics.cancer.gov/assay-portal/about/assay-characterization-guidance-documents). Tryptic peptides were selected to serve as molecular surrogates for the 270 target proteins according to a series of peptide selection rules (*e.g.*, sequence unique, devoid of oxidizable residues) and detectability, as described (25). All peptides were synthesized *via* Fmoc chemistry, purified through RP-HPLC with subsequent assessment by MALDI-TOF-MS, and characterized *via* amino acid analysis and capillary zone electrophoresis.

For CSF protein quantitation, new PRM assays targeting 325 proteins were developed for the present study. CSF protein targets were selected on the basis of three criteria. First, we compiled lists of proteins identified in rat and human CSF by our own previous proteomic analyses (16, 26). Second, we carried out an extensive literature review to identify proteins previously implicated in SCI or traumatic brain injury, or which had been proposed as biomarkers of another inflammatory central nervous system disease. Third, we conducted a pilot proteomic analysis of CSF from three patients. CSF samples were obtained from each patient at two timepoints (24 and 48 h post injury) and were analyzed in technical triplicate on a Bruker Impact II QTOF coupled to a Thermo Easy nLC-1000 through a house-packed 25 cm × 75 μm C18 column. The resulting dataset was searched using MaxQuant (26) at a 1% peptide and protein false discovery rate, and proteins identified in at least two patients were retained. Proteins identified by any of these three criteria were combined, and peptide targets from the resulting proteins were selected using PeptidePicker (27) on the basis of detectability by mass spectrometry, digestion efficiency, lack of potential modifications, lack of potential interferences, and conservation between human and pig. A total of 500 isotopically labeled peptides, containing either $^{13}C_6{}^{15}N_4$-Arg or $^{13}C_6{}^{15}N_2$-Lys on the C terminus of the peptide, were synthesized as above. These peptides were then individually validated for synthetic purity, detectability by mass spectrometry, and chromatographic performance. A total of 334 peptides were validated in this manner and were used for the remainder of the study. Collision energies and accumulation times were adjusted for individual peptides to provide optimal fragmentation (28) and adequate signal-to-noise ratios. High-quality tandem mass spectra were collected for each of these peptides, and a spectral library was produced containing all targets using Skyline (29). Both the serum (MRM) and CSF (PRM) assays corresponded to tier 2 assays, based on standards established by the National Cancer Institute's Clinical Proteomic Tumor Analysis Consortium Program (30).

Sample Processing

For serum samples, 10 μL of raw serum was subjected to 9 M urea, 20 mM dithiothreitol, and 0.5 M iodoacetamide, all in Tris buffer at pH 8.0. Denaturation and reduction occurred simultaneously at 37 °C for 30 min, with alkylation occurring thereafter in the dark at room temperature for 30 min. Proteolysis was initiated by the addition of TPCK-treated trypsin (35 μL at 1 mg/ml; Worthington) at a 20:1 substrate:enzyme ratio. After overnight incubation at 37 °C, proteolysis was quenched with 1% formic acid (FA). The stable isotope standard (SIS) peptide mixture was then spiked into the digested samples, the standard curve samples, and the QC samples and concentrated by solid phase extraction (Oasis HLB, 2 mg sorbent; Waters). After solid phase extraction, the concentrated eluate was frozen, lyophilized to dryness, and rehydrated in 0.1% FA (final concentration: 0.5 μg/μL digest) for LC-MRM/MS. For CSF samples, protein concentration was measured *via* Bradford assay, and one aliquot from each sample containing 200 μg of protein was prepared. Samples were lyophilized and resuspended in 25 mM ammonium bicarbonate, and protein concentrations were validated by a second Bradford assay. Proteins were digested with trypsin as described (31). A mix of all SIS peptide standards was added, and the sample was cleaned on C18 desalting columns (MacroSpin, Nest Group). The concentration of the SIS peptide mixture was chosen in order to produce a signal-to-noise ratio of at least 10:1. After C18 cleanup and drying, samples were resuspended in 60 μl of 0.1% FA.

Mass Spectrometry

For serum samples, 20-μL injections were separated with a Zorbax Eclipse Plus RP-UHPLC column (2.1 × 150 mm, 1.8 μm particle diameter; Agilent) contained within a 1290 Infinity system (Agilent). Peptide separations were achieved at 0.4 ml/min over a 60-min run, *via* a multistep LC gradient (2%–80% mobile phase B; mobile phase compositions: A was 0.1% FA in water, whereas B was 0.1% FA in acetonitrile). The column was maintained at 40 °C. A postgradient equilibration of 4 min was performed after each sample. The LC system was interfaced to a triple quadrupole mass spectrometer (Agilent 6490) *via* a standard-flow ESI source, operated in the positive ion mode. Peptide-specific LC-MS acquisition parameters were employed for optimal peptide ionization/fragmentation and scheduled MRM. Peptide optimizations were empirically optimized previously by direct infusion of the purified SIS peptides. Targets (one transition per peptide) were monitored over 500-ms cycles and 1-min detection windows.

For CSF samples, two 30-μL injections were performed serially, one with each of two PRM acquisition methods. The two methods had identical ionization, calibration, autosampler, and liquid chromatography conditions. Specifically, peptides were separated over a 70-min run, using LC gradients as above; the separation column was a 2.1 × 250 mm C18 Poroshell column (Agilent), held at 45°; the flow rate was 100 μL/min; and the ion source was the Agilent Jetstream ion source with reference mass calibration. The two methods differed in the peptide targets analyzed, with targets separated into the different methods based on retention time so as to minimize the number of concurrent eluting peptides analyzed per minute. Analysis of the CSF samples was performed on an Agilent 6550 QTOF mass spectrometer, coupled to an Agilent 1260 capillary flow HPLC, and an Agilent 1260 Autosampler.

To control for batch effects, pooled positive and negative control samples were aliquoted and equivalently loaded onto each plate. In addition, daily validations for instrument calibration and sensitivity, based on the *m/z* and intensity of heavy peptides, were performed by importing the data into Skyline and checking for intensity or *m/z* drift. Source cleaning, tuning, and calibrating were performed as needed.

Data Processing and Quality Control

Data from both serum and CSF samples was visualized and examined using Skyline (version 20.1.0.155) (29). This involved peak inspection to ensure accurate selection, integration, and uniformity (in terms of peak shape and retention time) of the SIS and natural peptide forms. In the serum, a standard curve was prepared using a mix of light peptides that was spiked into a human tryptic digest in which the peptides were dimethylated (to shift their masses) from a high concentration of 1000× the lower limit of quantitation (LLOQ) over eight dilutions to the lowest point of the curve, which was the LLOQ for the assay. The QC samples were prepared from the same light peptide mix and diluted in dimethylated human digest at 4×, 50×, and 500× the LLOQ for each peptide. After defining a small number of criteria

(*i.e.*, 1/x regression weighting, <20% deviation in the QC level accuracy) the standard curve was used to calculate the peptide concentration in fmol/μL in the patient samples through linear regression. Protein quantitations below or above the limit of quantitation were removed. In the CSF, peak ratios were calculated and extracted using the top six interference-free fragment ions that matched the library spectra. Protein quantitations were removed when the dot product to the library spectrum was less than 0.7 or the maximum peak height was below 20. Examples of raw MRM and PRM data with low, moderate, and high ratios are shown in supplemental Figure S1.

MRM and PRM proteomic data matrices were preprocessed by log-transformation, followed by correction of batch effects using the "removeBatchEffect" function in the R package "limma" (except in univariate analyses, where the batch was instead specified as a fixed effect in the linear model). Missing values were imputed as half of the lowest measured ratio or concentration for a subset of analyses that were unable to handle missing values, including principal component analysis, multivariate analysis, and all cross-species analyses; missing values were not imputed for the remainder of the analyses. For univariate and multivariate analyses, only proteins measured in at least one-third of samples were retained.

Modularity Analysis

Modularity analysis was performed essentially as described (32), using the R package "igraph" (33). Given a network and a grouping of nodes, modularity measures the degree to which nodes within each group are preferentially connected to one another. A weighted network was constructed in which nodes represent samples, and an edge was drawn between pairs of nodes when the Pearson correlation coefficient, computed across all proteins quantified in both samples, was higher than a given threshold. The modularity was subsequently computed with respect to several potential groupings of nodes (including patient, level of injury [cervical, thoracic, or lumbar], injury severity [baseline AIS grade], sex, or time post injury) as a function of network density, defined as the proportion of possible edges used to construct the network.

Univariate Analyses

Univariate analysis of protein abundance was performed using linear models with empirical Bayes shrinkage as implemented in the R package "limma" (18), and *p*-values were adjusted using Benjamini–Hochberg correction to control the false discovery rate. The plate on which each sample was stored and processed was included in all models in order to guard against the possibility of batch effects.

In the human dataset, associations between protein abundance and three clinical variables were evaluated: (i) injury status (*i.e.*, comparing samples from patients with acute SCI with uninjured controls); (ii) the severity of the initial injury, assessed using the AIS scale; (iii) recovery of motor function at 6 months post injury, quantified by the change in ASIA TMS (ΔTMS); and (iv) improvement in AIS grade at 6 months. Baseline AIS grade was modeled as an ordinal variable, ΔTMS as a continuous variable, and AIS grade improvement as a binary variable. Baseline neurological injury level (*e.g.*, C6 *versus* T9) was included as a covariate in models of 6-month ΔTMS and AIS grade improvement, in order to account for inherently different absolute potentials for motor recovery.

In the pig dataset, associations between protein abundance and four experimental variables were evaluated: (i) injury status (*i.e.*, comparing samples drawn from pigs after experimental SCI to matched samples from the same pigs at baseline); (ii) baseline injury severity, measured as the experimental injury severity group to which each pig was assigned; (iii) hindlimb neurological recovery, quantified using the average PTIBS score (20) across weeks 10 to 12 post injury; and (iv) white matter tissue sparing, quantified by histology at 12 weeks post injury. Baseline injury severity was modeled as a categorical variable, whereas hindlimb neurological recovery and white matter tissue sparing were modeled as continuous variables.

Consensus Clustering

k-Means consensus clustering was performed on the matrix of protein $\log_2$-fold change values over the first 5 days post injury, using the R package "ConsensusClusterPlus" (34). The Euclidean distance was used as the distance function, and 100 subsamples were performed. The change in the area under the cumulative distribution function was used to identify the optimal number of clusters, as the value of *k* at which there was no appreciable increase in the area under the cumulative distribution function. This procedure yielded a total of nine clusters in the CSF and eight in the serum. Of these, two in the CSF and one in the serum comprised two or fewer proteins and were removed, resulting in seven clusters of temporally coregulated proteins in each biofluid. Gene Ontology terms enriched within each cluster, relative to the remaining clusters, were identified using the conditional hypergeometric test (35) implemented in the R package "GOstats" (36).

Multivariate Analysis

We implemented an extensive pipeline to develop multivariate diagnostic and prognostic models using the python package scikit-learn (19), encompassing both parametric (*e.g.*, penalized logistic regression) and nonparametric (*e.g.*, gradient boosting machine) approaches. Specifically, for binary or multiclass classification tasks (including baseline AIS grade, baseline AIS A, change in TMS of seven or more points, AIS grade improvement, and motor complete injury at 6 months), we evaluated 12 different families of models, including Gaussian naive Bayes, *k*-nearest neighbors, nearest-centroid, support vector machine, logistic regression, linear discriminant analysis, random forest, extra trees, adaptive boosting, gradient boosting, and XGBoost classifiers. For the lone regression task, change in TMS at 6 months, we evaluated a further 11 families of models, including *k*-nearest neighbor, support vector machine, penalized logistic regression (with L1, L2, or elastic net penalties), L1-penalized least angle regression, random forest, extra trees, adaptive boosting, gradient boosting, and XGBoost regressors. We experimented with a number of different machine-learning approaches because no single method gives universally optimal results in practice, and it is difficult to predict *a priori* which model will be best suited to a particular task (37). Model performance in the discovery cohort was evaluated in 5-fold cross-validation. That is, each model was trained on 80% of the patients, and the trained model was then applied to make predictions for the remaining 20% of patients. This process was repeated five times, in order to make predictions for each patient in the discovery cohort. The metrics used to quantify model performance varied depending on the nature of the task. For binary classification tasks (for instance, AIS grade improvement), performance was evaluated using the accuracy and the area under the receiver operating characteristic curve (AUC). For multiclass classification tasks (for instance, baseline AIS grade), performance was evaluated using the accuracy and the balanced accuracy, which corrects for the baseline frequency of each class. For the lone regression task (change in TMS at 6 months post injury), performance was evaluated using the coefficient of determination. In cases where more than one model achieved optimal performance on a particular task, a single model was selected based on the other measure of performance (for instance, when two models achieved the same AUC, the model with the higher accuracy was retained) or at random, in cases of ties. Hyperparameter grids were adapted from Olson *et al*. (37), with minor modifications, and are provided in supplemental Tables S1 and S2. In addition to evaluating model hyperparameters, we also evaluated preprocessing choices, including

scaling and feature selection, using the scikit-learn "Pipeline" class. Feature selection was optionally performed by using limma to identify peptides with significant univariate associations to the clinical outcome of interest at nominal significance (that is, uncorrected $p < 0.05$) and was precalculated for each cross-validation fold in order to prevent inadvertent leakage of information between training and test splits. We additionally evaluated the impact of providing clinical data from the baseline neurological examination in conjunction with proteomic data, including age, sex, neurological level of injury, baseline AIS grade, baseline UEMS, baseline LEMS, and baseline AMS. Categorical features from the baseline neurological examination (baseline AIS grade and level of injury) were converted to binary indicator variables.

For the analysis of the validation cohort, the best models as determined by cross-validation in the discovery cohort were re-trained on the entirety of the discovery cohort and projected into the validation cohort to predict clinical outcomes. A total of six models were selected and preregistered for validation on the basis of the discovery cohort analysis. Samples from the validation cohort were blinded to investigators until the finalization of all statistical analyses of the discovery cohort, in order to provide an independent, blinded validation set.

Cross-species Analysis

Unless otherwise noted, all cross-species analyses were performed on a combined matrix of human and pig protein abundance including all proteins quantified in at least one-third of samples from either species, which was normalized by subtracting the mean and dividing by the standard deviation for each peptide separately within each species, as described (38). Modularity analysis was performed as described above, after restricting samples to those collected at four timepoints overlapping between species (24, 48, 72, and 120 h). The proportion of true null hypotheses, π_0, was estimated using the R package "qvalue" (39), from which the estimated proportion of true associations, π_1, was calculated as $1 - \pi_0$.

Rank–rank hypergeometric overlap analysis (40) was performed using the R package "RRHO." Briefly, after performing independent univariate analyses in either species as described above, all proteins quantified in either species were ranked by the strength and direction of DE, and a pair of sliding windows were passed along each of the two ranked lists. The hypergeometric probability of the observed overlap between proteins in each species was calculated for each pair of ranks. The statistical significance of each overlap was calculated by randomly permuting the status (*e.g.*, SCI *versus* control) of each human and pig sample, performing an identical univariate analysis with the permuted data, and comparing the maximum –log10 *p*-values achieved in 1000 permutations to the observed value (41).

Neighborhood analysis of conserved coexpression (NACC) (22) was performed to estimate the overall conservation of protein abundance patterns in SCI between species and to identify individual proteins or specific pathways with conserved or divergent patterns of abundance. Briefly, independent protein coexpression networks were constructed in either species, using the Pearson correlation coefficient to quantify similarity. The k nearest neighbors of each protein in turn were identified in the human coexpression network, and the mean correlation coefficient between the human neighbors and the protein of interest were calculated in pig. This procedure was repeated with human and pig inverted, and the average correlation across the two comparisons was retained as a symmetric measure of the degree of conservation of coexpression for each protein. We used a neighborhood size of $k = 10$ but found our conclusions robust to the neighborhood size. Permutation *p*-values (41) were calculated for each individual protein by comparing the observed NACC score to a distribution of NACC scores derived from 1000 random sets of "neighbors." An identical permutation test was applied to Gene Ontology (GO) terms annotated to between 3 and 50 proteins in both species, using the average NACC score of all genes within each GO category as the test statistic as described (22).

Dynamic time warping was performed using the R package "dtw" (42). Samples from uninjured controls and porcine samples collected at 12 weeks post injury were removed. Abundance profiles for each protein in either species were smoothed using a local polynomial filter to enhance time resolution (43), after which pairwise Euclidean distances were calculated between human and pig protein abundance at each pair of timepoints, and supplied as the local cost matrix to identify the optimal global alignment.

RESULTS

Overview of Study Cohorts

A total of 111 individuals sustaining an acute SCI were recruited through a multicenter prospective observational trial. Patients underwent a neurological examination at baseline, and again at 6 months post injury to determine the extent of neurological improvement. Clinical characteristics are provided in supplemental Table S3. CSF and serum samples were collected serially over the first 5 days post injury from all patients and were additionally obtained from 21 uninjured patients who served as negative controls. In total, 910 samples were collected and subjected to proteomic profiling, including 450 from the CSF and 460 from the serum, with between 63 and 100 samples from each biofluid collected at each timepoint (Fig. 1*A*).

In parallel, we conducted an experimental study in our previously described porcine model of traumatic SCI (20). The pig was selected on the basis of its anatomical and immunological similarities to human (44), in particular with respect to the dimensions of the spinal canal, which permit serial CSF collection through indwelling intrathecal ports (supplemental Fig. S2, *A* and *B*) (23). A total of 28 pigs received contusion SCIs of three different severities (mild, moderate, or severe; 9–10 pigs per group), and an additional 15 pigs received sham laminectomies (Fig. 1*B*). CSF and serum samples were collected 15 min prior to injury and serially over six timepoints between 12 h and 12 weeks post injury. Hindlimb neurological recovery was assessed weekly in all animals until 12 weeks, at which point animals were euthanized and spinal cords were collected for histological analysis (supplemental Fig. S2, *C–H*). In total, 419 samples were profiled from the pig study, including 204 from the CSF and 215 from the serum.

Development of Targeted Proteomic Assays for CSF and Serum

Accurate measurement of protein abundance in the CSF and serum is highly challenging, owing to the complexity and dynamic range of protein concentrations in these biofluids. In order to achieve sensitive and accurate protein quantitation, we leveraged targeted mass spectrometric strategies based on MRM in the serum and PRM in the CSF. In the serum, we took advantage of 270 existing MRM assays to target 270

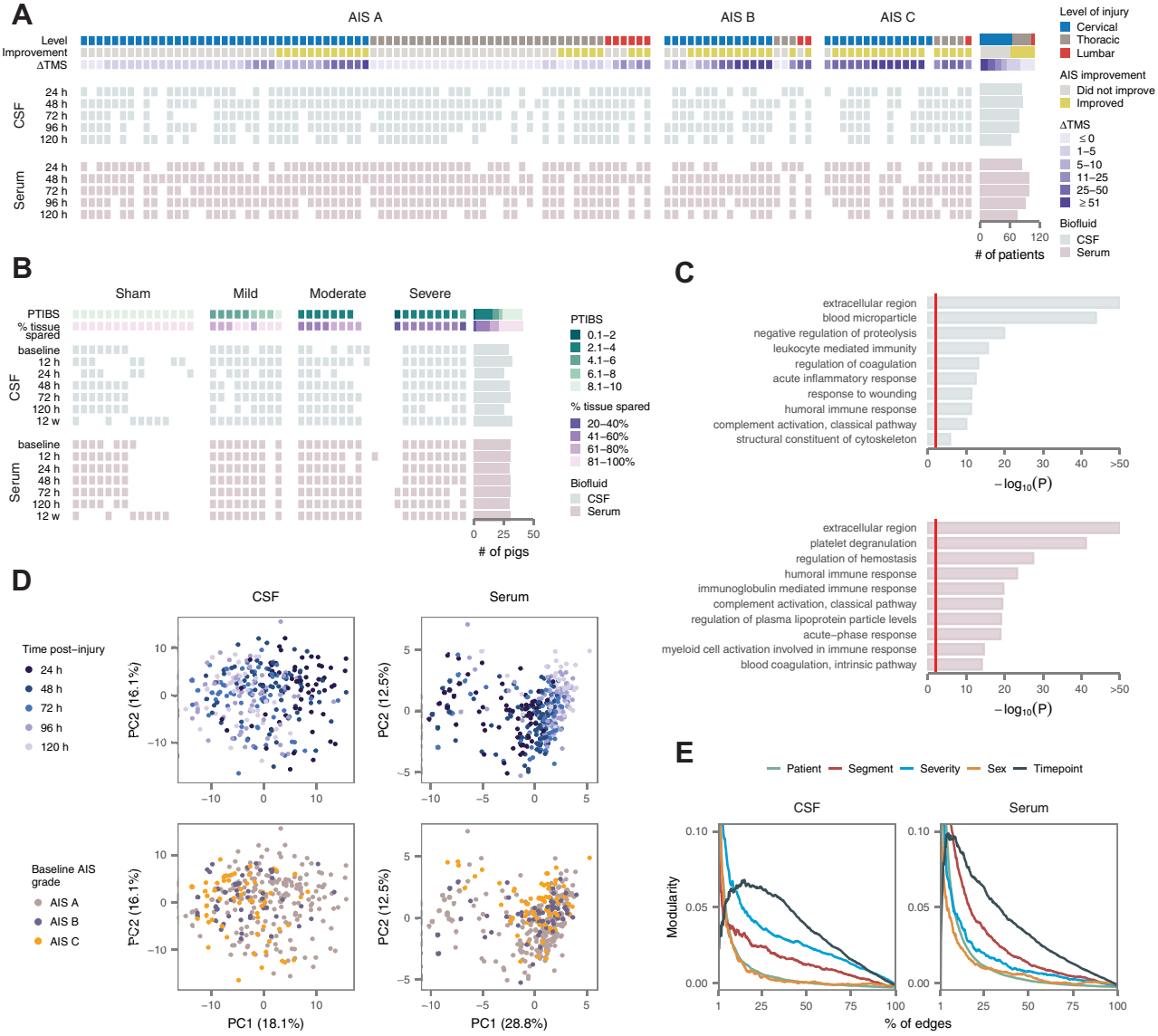

FIG. 1. **Targeted proteomic profiles of CSF and serum in human and pig spinal cord injury.** *A*, overview of the human cohort (*n* = 111 patients), including key clinical measures (level of injury, AIS conversion, and change in total motor score at 6 months post injury), *top*, and sample collection at each of five timepoints in the CSF, *middle*, and serum, *bottom*. *B*, overview of the pig cohort (*n* = 43 animals), including key experimental outcomes (Porcine Thoracic Injury Behavioral Scale score at 12 weeks post injury, percentage of histological tissue sparing), *top*, and sample collection at each of seven time points in the CSF, *middle*, and serum, *bottom*. *C*, Gene Ontology enrichment analysis of proteins targeted by synthetic peptides in the CSF, *top*, and serum, *bottom*. *Red line* shows $p = 0.01$. *D*, principal component analysis of human CSF and serum proteomes, with samples colored by time post injury, *top*, or baseline American Spinal Injury Association Impairment Scale (AIS) grade, *bottom*. *E*, modularity analysis of CSF and serum proteomes with samples grouped by patient, level of injury (cervical, thoracic, or lumbar spinal cord), injury severity (baseline AIS grade), sex, or time post injury. Modularity is shown as a function of the number of edges between samples used to construct the network, as a percentage of the total number of possible edges. CSF, cerebrospinal fluid

blood proteins, many of which have been previously been nominated as potential markers of other human diseases (24, 25). In the CSF, we developed new PRM assays for 334 peptides, targeting 325 distinct CSF proteins. Target proteins were selected for assay development on the basis of three criteria, including (i) identification in our own previous proteomics studies of rat or human CSF (16, 45); (ii) an extensive literature review to identify proteins previously implicated in SCI or traumatic brain injury, or which had been proposed as biomarkers of another inflammatory central nervous system disease; and (iii) pilot shotgun analyses of CSF from three patients. Together, the combination of the existing MRM assays and newly developed PRM assays afforded coverage of 491 unique proteins (supplemental Table S4*A*). GO terms

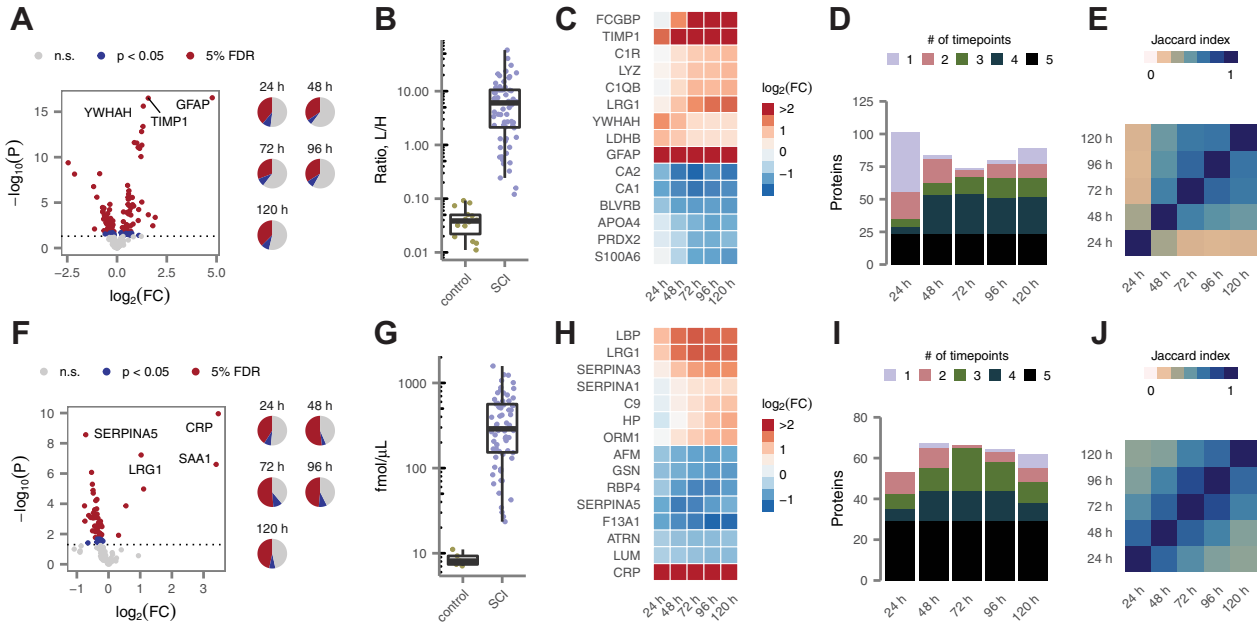

FIG. 2. **Profound alterations of the CSF and serum proteomes in acute SCI.** *A*, volcano plot of differential protein abundance at 24 h post injury in CSF samples from patients with acute SCI compared with uninjured controls. *B*, abundance of glial fibrillary acidic protein in CSF samples from patients with acute SCI and uninjured controls. *C*, time courses of differential protein abundance (log-fold change, relative to uninjured controls) over the first 5 days post injury for 15 of the most profoundly altered CSF proteins, based on the sum of $-\log_{10}$ *p*-values across all timepoints. *D*, number of differentially expressed CSF proteins at each of the first 5 days post injury in patients with acute SCI, grouped by the number of timepoints at which each protein was found to be differentially expressed. *E*, similarity of proteome alterations between all possible pairs of timepoints, as quantified by the Jaccard index between the differentially expressed proteins at each timepoint. *F*, as in (*A*) but showing differential protein abundance in the serum at 24 h post injury. *G*, abundance of C-reactive protein (CRP) in serum samples from patients with acute SCI and uninjured controls. *H–J*, as in (*C–E*), respectively, but showing serum proteins. CSF, cerebrospinal fluid; SCI, spinal cord injury.

enriched among proteins targeted by synthetic peptides reflected immunological and inflammatory pathways, cytoskeletal and secreted proteins, and coagulation (Fig. 1*C* and supplemental Table S4*B*). Isotopically labeled synthetic peptides were spiked into all samples at defined concentrations, allowing direct comparison of protein abundance across the study cohort. Technical reproducibility was high, with correlation coefficients of 0.96 and 0.99 between pooled controls in the CSF and serum, respectively (supplemental Fig. S3). The complete dataset of CSF and serum protein abundance data from both species is provided in supplemental Table S5.

Proteomic Portraits of SCI Across Tissues and Species

To obtain a global overview of the dataset, we first performed principal component analysis (PCA) of the human cohort. Samples separated on the first principal component by timepoint, rather than clinical severity, in both biofluids, suggesting that time post injury is the primary driver of variation in protein abundance following acute SCI (Fig. 1*D* and supplemental Fig. S4, *A* and *B*). Similar trends were apparent in analyses of the pig samples (supplemental Fig. S4, *C* and *D*).

To more formally quantify these trends, we constructed networks in both the serum and CSF, in which nodes corresponded to samples and edges were drawn between pairs of samples with correlated protein abundance, and carried out a modularity analysis of each network (32). Grouping samples by timepoint consistently yielded higher modularity than grouping by injury severity, confirming the trends observed visually by PCA (Fig. 1*E*). Of interest, in the serum, grouping by the injured spinal segment also yielded high modularity, suggesting the neurological level of injury shapes patterns of serum protein abundance within timepoints.

Profound Proteomic Alterations in Acute SCI

To date, interrogation of the molecular alterations that follow acute SCI has relied almost entirely on rodent models (46). Our large patient cohort provides an opportunity to define changes in the CSF and serum proteome of human SCI at a scale that has not previously been possible. We therefore first sought to characterize differential protein abundance following acute SCI (supplemental Table S6).

In the CSF, SCI caused profound changes in protein abundance. At 24 h post injury, 39% of targeted proteins displayed statistically significant differences relative to uninjured controls, at a 5% false discovery rate (FDR; Fig. 2*A*, left,

and supplemental Fig. S5*A*). Similar proportions of proteins were differentially expressed (DE) between 48 and 120 h (Fig. 2*A*, right). Many displayed dramatic alterations; for instance, the abundance of GFAP in the CSF differed by 25-fold between patients with SCI and controls (Fig. 2*B*).

Although a handful of the most significant associations were reproduced across all five timepoints, DE proteins displayed varying temporal patterns of up- or downregulation (Fig. 2*C* and supplemental Fig. S5*B*). For instance, GFAP was maximally upregulated immediately after injury, whereas complement proteins exhibited a delayed increase in abundance. Moreover, although most DE proteins were identified at a minimum of two adjacent timepoints, a substantial proportion were uniquely identified within 24 h of the initial injury (Fig. 2*D*). Using the Jaccard index to quantify the overlap in DE proteins over each of the first 5 days post injury, the 24-h timepoint emerged as a clear outlier (Fig. 2*E*). These observations suggest that a distinct set of pathophysiological processes are active in the spinal cord parenchyma during the most acute phase of the response to SCI.

Similarly marked changes were observed in the serum proteome after SCI, with 41% to 52% of proteins DE in patients with SCI over the 5-day time course (Fig. 2*F* and supplemental Fig. 5*C*). Acute-phase reactants such as C-reactive protein (Fig. 2*G*) were among the most strongly altered proteins. However, a less dramatic temporal course was apparent in the serum (Fig. 2*H* and supplemental Fig. S5*D*): most DE proteins were shared between adjacent timepoints, and the 24-h timepoint was not an obvious outlier (Fig. 2, *I* and *J*). These results suggest that the serum proteome reflects systemic responses to SCI that develop over longer timescales than those occurring within the central nervous system itself.

A unique aspect of our dataset is its time course design, whereby samples were collected serially from patients with acute SCI over the first 5 days post injury. In univariate analyses, nearly all proteins exhibited significant differences in abundance over this time course (supplemental Fig. S5*E*). To better understand the pathophysiological responses that are activated over the first 5 days after acute human SCI, we applied *k*-means consensus clustering (34) to identify modules of temporally coregulated proteins. Seven such modules were identified in each biofluid (supplemental Fig. S6, *A*–*D*). These included groups of proteins that were up- or downregulated immediately after injury but had returned to baseline by 5 days, as well as groups that displayed more delayed patterns of up- and downregulation, or which were up- or downregulated for the entire time course (supplemental Fig. S6, *E*–*H*). Analysis of enriched GO terms suggested functional correlates of each module (supplemental Fig. S6, *I* and *J*). Taken together, these analyses provide an initial description of the temporal profile of molecular changes in human CSF and serum following acute SCI.

Univariate Analysis Identifies Protein Biomarkers of SCI Severity and Recovery

Next, we sought to identify individual proteins whose abundance in the serum or CSF was associated with baseline injury severity, as quantified by the baseline AIS grade, or neurological recovery, as quantified either by the change in TMS (ΔTMS) or AIS grade improvement at 6 months post injury (supplemental Table S7). We initially focused on samples collected at 24 h. At this timepoint, a total of 23 proteins were associated with baseline AIS grade in the CSF, all of which were more abundant in patients with more severe injuries (Fig. 3*A*); the most statistically significant of these associations was to GFAP (Fig. 3*B*). Fourteen CSF proteins were significantly associated with ΔTMS (Fig. 3*C*), of which 11 were also associated with baseline AIS grade, including GFAP (Fig. 3*D*). After correction for multiple hypothesis testing, no proteins were associated with AIS grade improvement (Fig. 3*E*). In parallel analyses of serum samples collected at 24 h, only a single association was identified, between coagulation factor F11 (F11) and ΔTMS.

Given the dynamic temporal patterns of protein abundance observed in both biofluids, we subsequently repeated these analyses over each timepoint between 48 and 120 h. In the CSF, a total of 106 proteins were significantly associated with injury severity or neurological recovery within at least one timepoint (supplemental Fig. S7, *A*–*C*). We searched specifically for proteins with recurrent associations, spanning multiple timepoints or clinical outcomes, reasoning that these would be substantially less likely to represent spurious hits, and identified a total of 59 proteins with at least two statistically significant associations to injury severity or recovery (Fig. 3*F*). Among these, GFAP emerged as the most robust marker, with ten significant associations across all timepoints (Fig. 3*H*). The number of significant associations peaked at 48 h and subsequently declined, with none identified by 120 h (Fig. 3*H*). Associations to baseline AIS grade and change in TMS largely overlapped, but AIS grade improvement was reflected by a distinct proteomic signature (Fig. 3*I*).

We then carried out a parallel analysis of recurrently associated proteins in the serum (supplemental Fig. S7, *D*–*F*). Despite the dearth of associations at 24 h post injury, the serum proteome was substantially more informative with respect to clinical outcomes at later timepoints. A total of 24 proteins exhibited two or more statistically significant associations (Fig. 3*G*). As in the CSF, the number of associations to clinical outcomes peaked at 48 h, but a subset of serum proteins carried diagnostic or prognostic value as late as 120 h (Fig. 3*J*). Moreover, as in the CSF, there was substantial overlap between proteins associated with neurological recovery or baseline severity (Fig. 3*K*).

Together, these results define dozens of CSF and serum protein biomarkers with recurrent associations to injury severity or recovery over the first 5 days post injury and

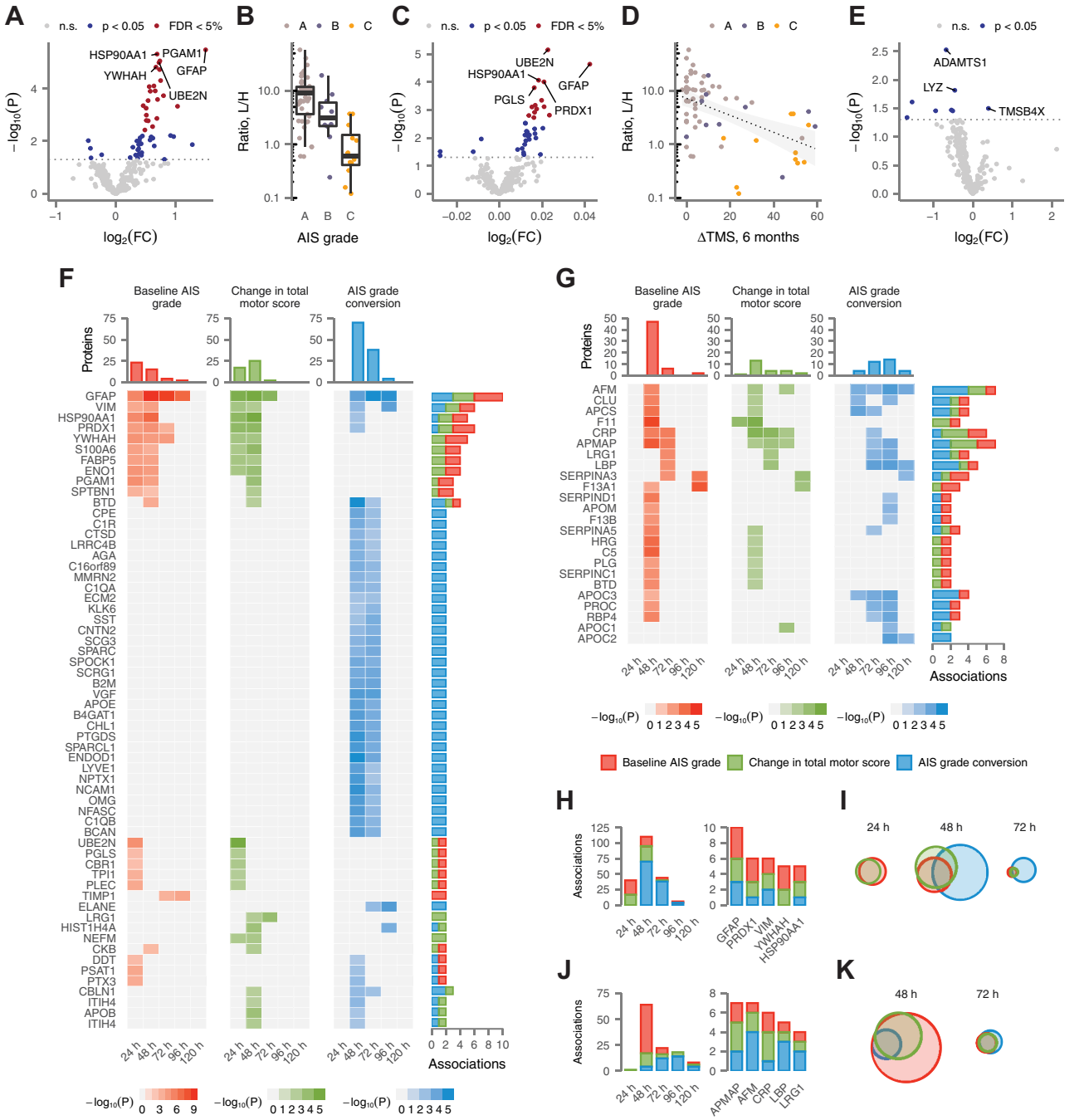

FIG. 3. **Univariate protein biomarkers of SCI severity and recovery.** *A*, volcano plot of differential protein abundance as a function of injury severity, as measured by the baseline AIS grade, in CSF samples at 24 h post injury. *B*, abundance of glial fibrillary acidic protein (GFAP) in CSF samples from patients with acute SCI, stratified by baseline AIS grade. *C*, volcano plot of differential protein abundance as a function of neurological recovery, as measured by the change in total motor score at 6 months post injury, in CSF samples at 24 h post injury. *D*, abundance of GFAP in CSF samples from patients with acute SCI compared with change in total motor score at 6 months post injury. *E*, volcano plot of differential protein abundance as a function of neurological recovery, as measured by AIS grade improvement over baseline at 6 months post injury, in CSF samples at 24 h post injury. *F*, statistical significance of associations between CSF protein abundance and three clinical outcomes over the first 5 days post injury for 59 proteins with two or more significant associations. *Gray squares* indicate associations that were not significant after correction for multiple hypothesis testing. *G*, as in (*F*) but for 24 serum proteins with two or more significant associations. *H*, number of statistically significant associations between CSF protein abundance and three clinical outcomes per timepoint, *left*, and for the five CSF proteins with the most recurrent associations, *right*. *I*, overlap between CSF proteins significantly associated with three clinical outcomes at 24, 48, and 72 h post injury. *J*, as in (*H*) but for serum proteins. *K*, as in (*I*) but for serum proteins at 48 and 72 h. AIS, American Spinal Injury Association Impairment Scale; CSF, cerebrospinal fluid; SCI, spinal cord injury.

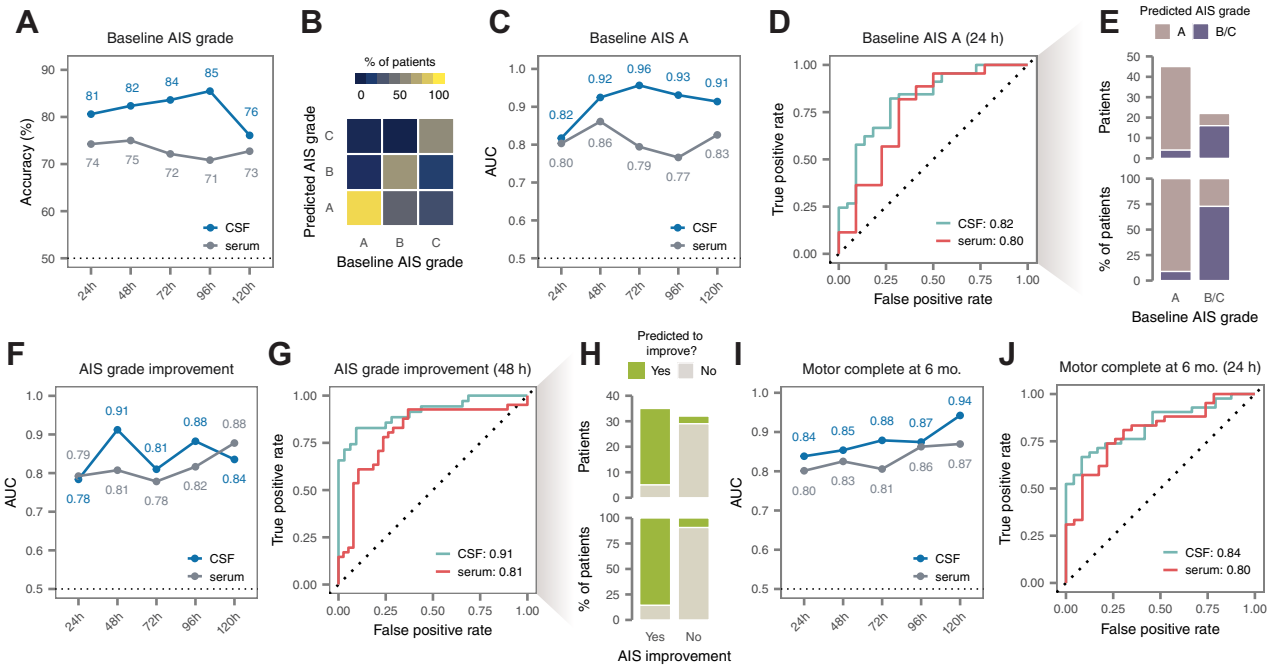

FIG. 4. **Multivariate protein biomarkers of spinal cord injury severity and recovery.** *A*, cross-validation accuracy of multivariate diagnostic models trained to stratify patients by baseline AIS grade, at timepoints between 24 and 120 h post injury. *B*, confusion matrix of the best CSF diagnostic model of baseline AIS grade at 48 h post injury. *C*, cross-validation AUC of multivariate diagnostic models trained to discern patients with a baseline AIS grade of A, at timepoints between 24 and 120 h post injury. *D*, ROC curves of the best CSF and serum diagnostic models at 24 h post injury. *E*, predictions made by the best CSF diagnostic model at 24 h post injury. *F*, cross-validation AUC of multivariate prognostic models trained to predict improvement in AIS grade at 6 months post injury, relative to baseline, at timepoints between 24 and 120 h post injury. *G*, ROC curves of the best CSF and serum prognostic models of AIS grade improvement at 48 h post injury. *H*, predictions made by the best CSF prognostic model at 48 h post injury. *I*, cross-validation AUC of multivariate prognostic models trained to predict motor complete *versus* incomplete injury at 6 months, at timepoints between 24 and 120 h post injury. *J*, ROC curves of the best CSF and serum prognostic models of motor complete *versus* incomplete injury at 24 h post injury. AIS, American Spinal Injury Association Impairment Scale; AUC, area under the receiver operating characteristic curve; CSF, cerebrospinal fluid; ROC, receiver operating characteristic.

suggest that protein abundance at 48 h generally carries the greatest prognostic value.

Machine Learning Defines Highly Accurate Multiprotein Diagnostics

Next, we sought to optimize the accuracy of patient stratification or prognostication by combining diagnostic or prognostic information across multiple proteins simultaneously, through multivariate analyses. To this end, we developed a comprehensive machine learning pipeline, implementing a total of 22 different classification and regression models. We then applied this pipeline to CSF and serum proteomics data from each timepoint (supplemental Table S8).

We first directed our machine learning pipeline to develop multiprotein diagnostic models of baseline AIS grade. Models trained on CSF protein concentrations at 24 h or 48 h both achieved good accuracy in 5-fold cross-validation (81% and 82%, respectively; Fig. 4*A*). However, the balanced accuracy, which adjusts for differences in the prevalence of each AIS grade, was substantially higher at 48 h (72% *versus* 65%; supplemental Fig. S8*A*). Closer inspection suggested that both models had difficulty correctly identifying AIS B patients (Fig. 4*B* and supplemental Fig. S8*B*). Serum models were generally less accurate (Fig. 4*A*, supplemental Fig. S8, *A* and *C*). Although the severity of the injury is likely to be clinically apparent by 48 h in individuals able to perform a baseline neurological examination, a substantial proportion of patients remain poorly examinable up to 72 h post injury, owing to intubation and sedation following urgent surgical intervention. These patients would conceivably be candidates for emerging therapies delivered at subacute timepoints, suggesting that a diagnostic tool based on CSF protein abundance at 48 h could have substantial clinical utility.

Motivated by the observation that our diagnostic models struggled to differentiate intermediate injury severities, we also asked whether we could specifically discriminate AIS A from AIS B or C patients. Indeed, CSF models demonstrated strong performance in identifying AIS A patients as early as 24 h, achieving a maximum AUC of 0.82 and an accuracy of 85% (Fig. 4, *C–E* and supplemental Fig. S8*D*). Performance was only slightly poorer in the serum (Fig. 4, *C* and *D*). These findings suggest the possibility of an acute diagnostic test to

specifically identify the subset of patients in whom the likelihood of spontaneous recovery is the lowest.

Multiprotein Biomarkers Predict Neurological Improvement at 6 Months Post Injury

Next, we applied the same machine learning pipeline to develop multiprotein models capable of prognosticating ultimate neurological recovery. With respect to ΔTMS, the best performance was achieved by a model trained on the CSF proteome at 48 h, which achieved a coefficient of determination (r^2 score) of 0.51 (supplemental Fig. 8, *E* and *F*). However, performance was poorer for CSF models at 24 h, and in the serum at either timepoint. Previous studies have defined ΔTMS beyond a prespecified threshold, typically 6 to 7 points, as a primary outcome (47, 48), and consequently we investigated whether better accuracy could be achieved in predicting a ΔTMS of 7 or greater. Indeed, we found that serum models achieved an AUC of 0.83 and an accuracy of 78% at 24 h on this task (supplemental Fig. S8, *G–I*). Thus, although predicting the exact magnitude of the change in TMS is challenging, predicting whether there will be a clinically meaningful improvement can be achieved with reasonably good accuracy.

We also sought to predict neurological recovery as defined by improvement in the AIS grade, another measure that has widely been used as a primary endpoint in clinical trials (49, 50) (Fig. 4*F* and supplemental Fig. S8*J*). The best-performing models made use of CSF proteomics data at 48 h post injury, achieving an exceptionally high AUC of 0.91 and an accuracy of 88% (Fig. 4, *G* and *H*). This performance suggests the possibility of highly accurate identification of patients likely to demonstrate spontaneous neurological improvement, with implications for both the design of clinical trials and acute patient management. The performance of the single best model at 48 h was not significantly greater than that of the top-performing models at 24 or 72 h, with AUCs of 0.78 and 0.81, likely due to the size of the cohort ($p = 0.06$ and 0.13, respectively, DeLong test). However, models on average attained higher AUCs at 48 h than at 24 or 72 h ($p = 0.008$ and 0.0006, *t* test), suggesting that the CSF proteome may generally contain more prognostic signal at this timepoint.

In view of these successes, we further evaluated the possibility of directly prognosticating neurological impairment at 6 months. Prediction of 6-month AIS grade was not substantially better than random expectation (supplemental Fig. S8*K*). However, we found that multiprotein models could reliably distinguish motor complete *versus* incomplete injuries at 6 months (that is, a 6-month AIS grade of A/B *versus* C/D; Fig. 4*I* and supplemental Fig. S8*L*). At 24 h, the best serum model achieved an AUC of 0.80 and an accuracy of 80% (Fig. 4*J* and supplemental Fig. 8*M*).

Taken together, these results suggest that it is possible to predict much of the observed variation in neurological recovery at 6 months post injury on the basis of protein abundance in acutely collected CSF and serum samples.

Validation of Single- and Multiprotein Biomarkers in an Independent Clinical Cohort

Having established both single- and multiprotein biomarkers of SCI severity and recovery, we next sought to validate these in an independent clinical cohort (supplemental Table S9). Samples from the validation cohort ($n = 20$ patients) were processed separately from the discovery cohort and blinded to investigators until after finalization of all statistical analyses. A large fraction of the alterations following acute SCI were reproduced within each biofluid and timepoint, and effect sizes were highly correlated between cohorts for proteins with reproducible alterations ($r \geq 0.90$; Fig. 5, *A–D* and supplemental Fig. S9, *A–D*). A total of 28 associations to injury severity or recovery were reproduced at 5% FDR, with a further 30 nominally significant (Fig. 5, *E* and *F*). In the CSF, GFAP again stood out as the most promising candidate, with six associations validated at nominal significance or better (supplemental Fig. S9, *E–G*). In the serum, associations between LRG1 at 72 h and both ΔTMS and AIS grade improvement were reproduced at 5% FDR (supplemental Fig. S9, *H* and *I*).

Among the multivariate models described above, six were selected and preregistered for validation, including four CSF and two serum models. All four CSF models achieved performance comparable with that observed in the discovery cohort (Fig. 5*G*); serum models, in contrast, did not demonstrate convincing accuracy (supplemental Fig. S9*J*). Remarkably, in the validation cohort, patients with a baseline AIS grade of A could be identified with an AUC of 0.93 from 24 h CSF (Fig. 5*H*) and AIS grade improvement at 6 months could be predicted with an AUC of 0.88 from 48 h CSF (Fig. 5*I*). Models of baseline AIS grade and ΔTMS based on 48 h CSF also achieved good performance (supplemental Fig. S9, *K* and *L*). Although not among the six preregistered models, we additionally observed that patients with motor complete injuries at 6 months could be identified from 24 h CSF with an AUC of 0.96 in the validation cohort (supplemental Fig. S9*M*).

Thus, through blinded evaluation in an independent cohort, enrolled and processed after the discovery cohort to emulate a prospective clinical study, we successfully validated dozens of individual proteins and four multiprotein models for patient stratification and prognostication in SCI.

Proteomic Alterations in a Large Animal Model of SCI

The vast majority of our knowledge concerning the pathophysiological responses to acute SCI has emerged from studies in animal models. Through these studies, many therapies have emerged that effectively target the secondary injury responses triggered after SCI in rodents and other species. However, the subsequent failure of these apparently promising agents in human clinical trials raises the possibility

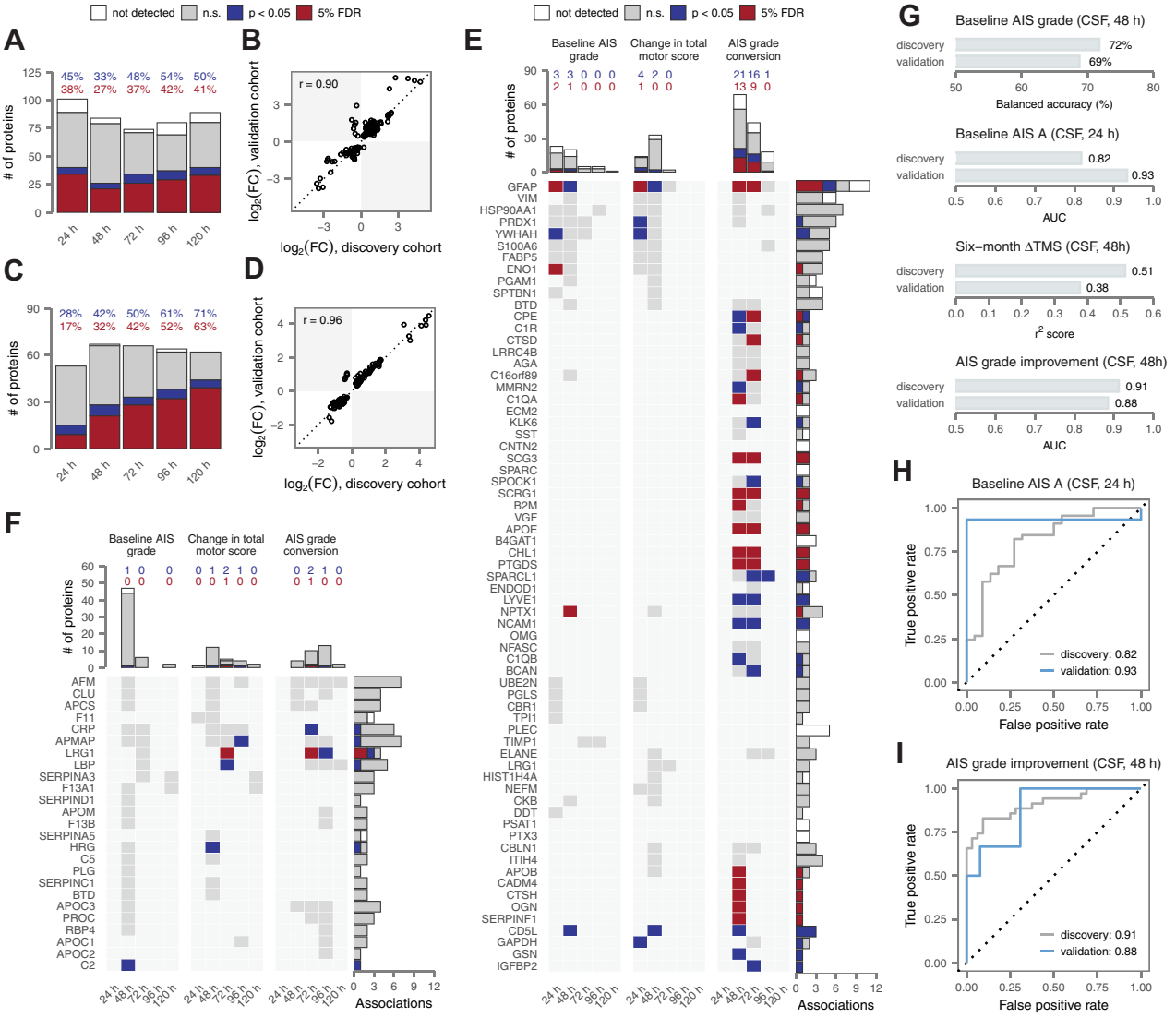

FIG. 5. **Validation of univariate and multivariate biomarkers in an independent cohort.** *A*, replication of univariate alterations in CSF protein abundance after acute SCI. Bar graph shows the total number of differentially abundant proteins that were replicated at nominal significance or after multiple hypothesis testing correction, were not significant, or were not quantified in the validation cohort. Inset text shows the proportion of differentially abundant proteins that were replicated at nominal significance (*blue*) or after multiple hypothesis testing correction (*red*). *B*, correlation between $\log_2$-fold changes between the discovery and validation cohorts for proteins with replicated alterations. *C* and *D*, as in (*A* and *B*) but for alterations in serum protein abundance. *E*, replication of associations between CSF protein abundance and three clinical outcomes over the first 5 days post injury for 59 proteins with two or more significant associations (as shown in Fig. 3*F*) and an additional eight proteins with a single association replicated with at least nominal significance. Inset text shows the total number of associations that were replicated at nominal significance (*blue*) or after multiple hypothesis testing correction (*red*). *F*, as in (*E*) but for the 24 serum proteins with two or more significant associations (as shown in Fig. 3*G*) and one additional protein with a single association replicated with nominal significance. *G*, performance of four preregistered multivariate CSF models in an independent validation cohort. *H*, receiver operating characteristic curves of the best CSF diagnostic model of AIS A patients at 24 h post injury (as shown in Fig. 4*D*) in the discovery and validation cohorts. *I*, receiver operating characteristic curves of the best CSF prognostic models of AIS grade improvement at 48 h post injury (as shown in Fig. 4*G*) in the discovery and validation cohorts. AIS, American Spinal Injury Association Impairment Scale; CSF, cerebrospinal fluid.

that important biological differences exist between animal models and human SCI. The difficulty of translating novel therapies is compounded by the fact that functional or anatomical outcome measures assessed in animal models, such as "hindlimb locomotor function" or "white matter sparing at the injury site," cannot be measured in humans, or may have limited relation to clinically relevant outcomes. Establishing biochemical markers that are predictive of neurological outcomes in both animal models and human patients could provide endpoints for preclinical studies that

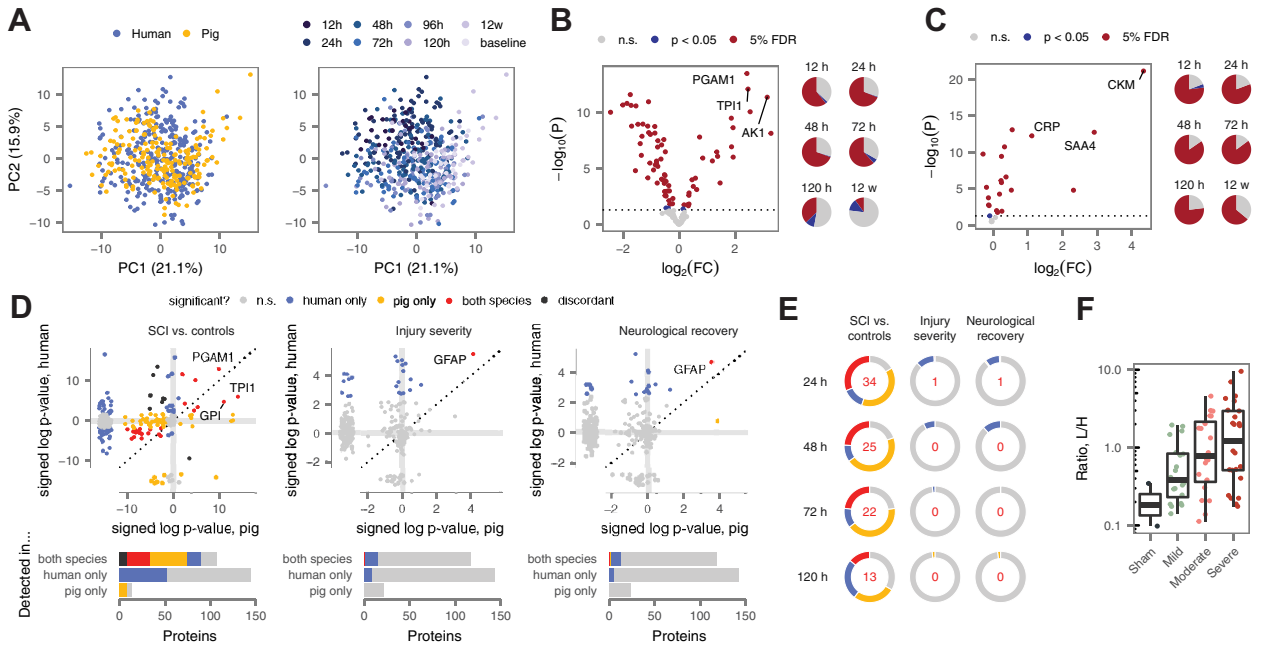

FIG. 6. **Proteomic profiles of a large animal model define cross-species biomarkers of SCI.** *A*, principal component analysis of human and pig CSF proteomes, with samples colored by species, *left*, or time post injury, *right*. *B* and *C*, volcano plots of differential protein abundance at 24 h post injury in CSF (*B*) and serum (*C*) samples from injured pigs, compared with samples drawn from the same pigs at baseline (15 min prior to injury). Pie charts show the proportion of differentially expressed proteins between 12 h and 12 weeks post injury. *D*, *top*, signed $-\log_{10}$ *p*-values for differential protein abundance at 24 h in human and pig, in comparisons of individuals with acute SCI and uninjured controls, *left*; as a function of injury severity, *middle*; or as a function of neurological recovery, *right*. Marginal plots show *p*-values for proteins quantified in human (pig) only. *Bottom*, number of proteins with statistically significant differential abundance in both species, human only, pig only, or neither, among proteins quantified in both species, human only, or pig only. *E*, proportion of human and pig proteins that are differentially abundant in both species, one species, or neither, at all four matched timepoints following acute SCI, *left*; as a function of injury severity, *middle*; or as a function of neurological recovery, *right*. Inset numbers show proteins that were differentially abundant in both species. *F*, abundance of GFAP in pig CSF samples at 24 h post injury as a function of injury severity. CSF, cerebrospinal fluid; GFAP, glial fibrillary acidic protein; SCI, spinal cord injury.

are directly informative about human SCI. We therefore sought to leverage our parallel study of SCI in a large animal model in order to identify biochemical markers of injury severity and recovery that could serve as translational linkages between species.

We first addressed whether, in a combined analysis of human and pig samples, proteomic profiles would segregate globally by species or by time post injury, the dominant source of within-species variation. To this end, we performed PCA on a combined matrix of human and pig samples at four matching timepoints (24, 48, 72, and 120 h). Reassuringly, samples separated primarily by time post injury, rather than by species, suggesting that divergences between species are not so pronounced as to preclude extrapolation from one organism to another (Fig. 6*A*). Modularity analysis quantitatively confirmed this trend (supplemental Fig. S10*A*). Parallel analyses yielded similar results in the serum (supplemental Fig. S10, *B* and *C*).

Having established a basis for cross-species comparison, we next sought to identify differences in protein abundance between CSF and serum samples collected from injured pigs and matching samples drawn 15 min prior to injury (supplemental Table S10). Despite the comparatively lower number of observations in pig (n = 25–32 samples per biofluid and timepoint), this repeated-measures design provided excellent statistical power to detect proteomic alterations in SCI, with 37% to 69% of proteins DE over the first 5 days post injury (Fig. 6, *B* and *C* and supplemental Fig. S10, *D*–*G*). Several of these changes persisted until 12 weeks post injury, providing an initial description of proteomic alterations in the chronic phase of SCI. Similarly, we performed univariate analyses of baseline severity, neurological recovery, and histological tissue sparing in the pig CSF and serum, identifying 13 proteins with recurrent associations to experimental variables in the CSF and four in the serum (supplemental Fig. S10, *H* and *I*). The majority of these associations were detected at 12 h, although a subset were detected over multiple timepoints (supplemental Fig. S10, *J* and *K*).

We next took advantage of our parallel univariate analyses in both human and pig to directly compare protein alterations across species, focusing our analysis primarily on the CSF due to the relatively small number of associations in the serum of either species. A substantial fraction of CSF proteins were comparably modulated following SCI in both human and pig, with 14% to 31% of proteins DE in both species at matching timepoints (Fig. 6, *D* and *E* and supplemental Fig. S11*A*).

Accounting for incomplete power by using the π_1 statistic to estimate the proportion of null hypotheses (27) further increased the estimated degree of overlap, to 57 to 81% (supplemental Fig. S10, *L* and *M*).

These data indicated that the proteomic alterations that accompany acute SCI are broadly conserved between human and pig. In contrast, markers of injury severity or recovery were more species specific. Across all four matching timepoints, only two associations were reproduced in both species (Fig. 6*E* and supplemental Fig. S11, *B–D*). Remarkably, these implicated the same protein at the same timepoint: CSF levels of GFAP at 24 h were correlated to both baseline injury severity and hindlimb neurological recovery in pigs (Fig. 6*F* and supplemental Fig. S10*N*). Thus, despite differences in markers of severity or recovery across species, this finding raises the possibility that GFAP levels in the CSF could provide a biochemical outcome measure that could be used to monitor injury progression and therapeutic response in animal studies, with direct relevance to human injury.

Convergent Proteomic Signatures in Human and Porcine SCI

Although univariate analyses successfully identified individual proteins altered in both human and pig SCI, we reasoned that relying on a simple overlap between DE proteins in either species could reduce our sensitivity to detect small but concordant changes. To overcome this limitation, we performed a threshold-free analysis using rank–rank hypergeometric overlap (RRHO) (40) to identify convergent proteomic signatures of acute SCI, injury severity, and recovery. We applied this method to compare all pairs of timepoints evaluated in either species, reasoning that equivalent responses may not be activated at perfectly matching timepoints between species.

We first applied RRHO analysis to compare proteomic signatures of acute SCI (Fig. 7*A*). As anticipated from our univariate analyses, highly significant overlap was observed between approximately matching timepoints (Fig. 7*B*). Surprisingly, however, there was more limited overlap between mismatched timepoints, suggesting substantial dynamic evolution in the molecular response to SCI over the first 5 days post injury. The greatest overlap was observed at 24 h and earlier, indicating the most acute phase of the response to SCI is the most strongly conserved between species. Subacute and chronic phases also showed a broad alignment, with significant overlap between the human protein signature of SCI at 120 h and the pig signature between 72 h and 12 weeks. This observation suggests that many of the molecular alterations that persist into the chronic stage of the injury have been established in human by 120 h post injury.

We next applied RRHO to compare protein signatures of injury severity and neurological recovery (Fig. 7*B* and supplemental Fig. S12*A*). Broadly similar patterns to those identified for acute SCI were observed in the latter analysis, with the strongest overlap at the most acute stages of injury, and a more modest overlap at 120 h. In contrast, no significant overlaps were detected between human and pig with respect to baseline injury severity (supplemental Fig. S12*B*). This finding may reflect a fundamental dissimilarity between the precisely controlled measures of injury severity employed in animal studies and the subjective, ordinal assessments carried out in the emergency room.

Conserved and Divergent Patterns of Protein Coexpression

Beyond comparing signatures of specific clinical outcomes, we sought to identify individual proteins or biological processes with diverging patterns of abundance across species more generally. To this end, we applied neighborhood analysis of conserved coexpression (NACC) (22). This method has the advantage of not requiring that samples from either species be precisely matched with respect to clinical outcomes or timepoints, so long as two large and diverse panels are provided.

To apply NACC, we constructed protein coexpression networks in the CSF of either species and evaluated the degree to which proteins tended to be coexpressed with the same neighbors across species. On a global level, we observed a significantly higher degree of shared coexpression between species than random expectation ($p < 10^{-15}$, Brunner–Munzel test; Fig. 7*C*), providing further evidence for broad conservation of protein function in SCI. Using the π_1 statistic, we estimated that 82% of proteins are coexpressed with shared neighbors across species (Fig. 7*D* and supplemental Fig. S12*C*). Ranking individual proteins based on the strength of conservation of their coexpression neighborhood (Fig. 7*E* and supplemental Table S11*A*), we found that no individual protein exhibited a significant divergence across species.

We then performed a similar NACC analysis at the level of biological processes. Among 220 GO terms robustly quantified in both species, 8 were significantly conserved, whereas 9 were divergent (Fig. 7*F* and supplemental Table S11*B*). GO terms displaying significantly conserved coexpression were largely related to neuronal structure and function (*e.g.*, “axon guidance,” “glutamatergic synapse”). Conversely, GO terms associated with evolutionary divergence implicated immune and inflammatory processes (“immune response,” “cellular response to tumor necrosis factor”). Taken together, these analyses indicate broad conservation of protein function but evolutionary divergence in the immune response to SCI.

Temporal Deviations in the SCI Response Across Species

Preclinical studies in animal models often proceed from the implicit assumption that administering a therapeutic intervention at a particular timepoint in an animal model will elicit comparable effects at the same timepoint in humans. To directly address the possibility that comparable biological

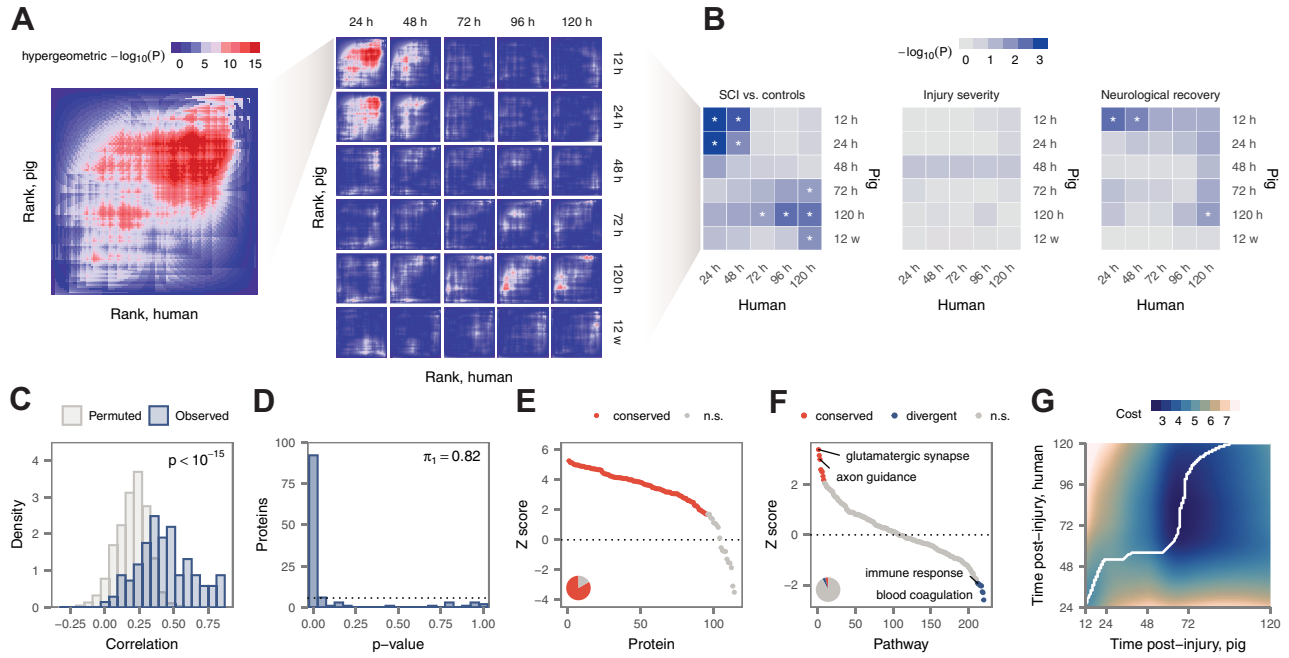

FIG. 7. **Evolutionary conservation of the proteomic response to SCI**. *A*, overview of the RRHO approach, comparing human and pig differential protein abundance after acute SCI. *Left*, RRHO plot comparing ranked lists of differentially abundant proteins at 24 h (human) and 12 h (pig) as an illustrative example. Rows and columns show the number of top-ranked proteins from human and pig, respectively, used to calculate the hypergeometric *p*-value. *Right*, RRHO plots for all pairs of timepoints in human and pig. *B*, RRHO comparisons of differential protein abundance between human and pigs after acute SCI, *left*; as a function of baseline injury severity, *middle*; and as a function of neurological recovery, *right*. Asterisks denote comparisons with $p < 0.05$. *C*, distribution of NACC scores for proteins in human and pig samples, compared with randomly selected neighbor proteins. *D*, distribution of NACC score permutation *p*-values for individual proteins between human and pig. *E*, ranked NACC score z-scores for individual proteins, with significantly conserved proteins *highlighted*. Inset pie chart shows the total proportion of significantly conserved proteins. *F*, ranked NACC score z-scores for Gene Ontology functional categories, with significantly conserved pathways *highlighted*. Inset pie chart shows the total proportion of significantly conserved and divergent pathways. *G*, local cost matrix for the temporal alignment of human and pig CSF proteomes over the first 5 days post injury by dynamic time warping; *white line* shows the optimal alignment. NACC, neighborhood analysis of conserved coexpression; RRHO, rank–rank hypergeometric overlap; SCI, spinal cord injury.

processes are activated at different timepoints in animal models, we applied dynamic time warping to temporally align the proteomes of both species over the first 5 days post injury (Fig. 7*G*). Intriguingly, we found that the two time courses were not directly aligned. Early timepoints in pig aligned to slightly later timepoints in human, suggesting that key aspects of the response to acute SCI progress faster in pig. This finding is consistent with RRHO analysis (Fig. 7*B*), where the strongest overlaps were observed between 12 h in pig and 24 h in human, and was further supported by inspecting alignments of individual proteins (supplemental Fig. S12*D*). For instance, the concentration of CKB in pig CSF decreases to a low at approximately 48 h, before returning to higher concentrations by 120 h (supplemental Fig. S12*E*); in humans, CKB had not yet returned to its initial concentration by 120 h. These observations provide systematic molecular evidence that the dynamics of the SCI response are not directly aligned between human patients and a large animal model, with particular implications for the neuroprotective agents that might be tested during the most acute phase of injury.

DISCUSSION

Despite the emergence of several promising therapeutic approaches in preclinical studies, clinicians presently lack effective treatments to restore function in acute SCI. In this work, we sought to address a number of factors underlying the translational divide in SCI through proteomic analyses of CSF and serum from 111 patients with acute SCI and, in parallel, from a large animal model. Through our analysis of this dataset, we aimed to (i) enhance our basic understanding of the pathophysiology of acute human SCI, (ii) develop diagnostic and prognostic biomarkers of neurological impairment, and (iii) establish biological commonalities and differences between human SCI and a large animal model. Our findings have a number of implications for basic, translational, and clinical research in SCI.

Over the course of several decades, small-scale studies of SCI in animal models, primarily rodents, have amassed a substantial body of understanding about the pathobiology of SCI. In contrast, direct observations of secondary injury responses in human patients have historically been rare and limited both by

sample size and the number of analytes measured (13–17, 51, 52). The paucity of molecular-level descriptions of human SCI presents a broad limitation for translational research in a field that relies almost entirely on rodent experimental models for the development of new therapies. In this context, our analysis of 491 proteins across a total of 844 samples from 111 patients with acute SCI provides an unprecedented resource to understand the evolving molecular responses to human SCI over the first 5 days post injury, both within the central nervous system and systemically. Moreover, through serial collection of both biofluids over the first 5 days post injury, we characterized the temporal profile of molecular changes following acute SCI, allowing us to dissect the complex biological responses that unfold over time after traumatic injury. Strikingly, we found that the proteomic alterations during the most acute phase, up to 24 h post injury, were substantially distinct from those over the subsequent 4 days. This observation is particularly noteworthy given that our cross-species analysis established these early responses as most strongly conserved across species and thus reveals an evolutionarily conserved "hyper-acute" phase of SCI.

A primary goal of our study was to establish diagnostic and prognostic biomarkers of SCI. Through univariate analyses, we identified dozens of CSF and serum proteins with recurrent associations to injury severity or recovery, among which GFAP emerged as a particularly promising candidate. We then applied a machine learning pipeline to develop multiprotein models. Perhaps most remarkably, we established a prognostic model capable of predicting AIS grade improvement at 6 months from the CSF proteome at 48 h post injury with an AUC of 0.91. Excellent performance was also achieved in stratifying patients by AIS grade, identifying AIS A patients, and predicting motor complete injuries at 6 months. We subsequently went on to validate both univariate markers and preregistered multivariate models in an independent clinical cohort, in a manner designed to rigorously emulate a prospective clinical evaluation. To this end, patients in the validation cohort were consecutively enrolled after the discovery cohort had been finalized, and all sample preparation and data acquisition occurred separately for these patients. Moreover, investigators were blind to the validation cohort data until finalization of all statistical analyses in the discovery cohort and a small number of multiprotein models were preregistered for validation. Previous attempts to identify biomarkers in acute SCI have generally taken place in small patient cohorts, lacked validation in an independent cohort, and in several cases conflated training and test data when reporting accuracy. The methodological rigour of our efforts to validate these markers thus goes substantially beyond what has previously been achieved in this field. The success of this effort indicates that these tools could both facilitate the conduct of clinical trials and inform decisions about acute and rehabilitative management, setting the stage for eventual precision medicine approaches.

The degree to which widely used animal models accurately reflect the pathophysiological processes active in SCI, and human disease more generally, has been extensively debated (53–56). Through comparative proteomic analysis in a porcine model, we provide systematic molecular evidence of substantial concordance in the molecular response to SCI between species, with several orthogonal analyses converging on an estimate that ~80% of proteome alterations are shared between human and pig. However, we also detected divergence in specific processes, most notably the immune response. We identified convergent proteomic signatures of neurological recovery, but not injury severity, possibly reflecting a fundamental dissimilarity between measures of severity employed in human and animal studies. Our search for conserved biological endpoints nonetheless led to the identification of GFAP as significantly correlated to both baseline severity and neurological outcome in both species. Last, our dense time course design in either species allowed us to perform, to our knowledge, the first systematic comparison of temporal patterns in the molecular response to a disease between species. Through a direct alignment of the human and pig time courses, we identified accelerated progression of the SCI response in our pig model, with implications for the timing of drug administration or other therapeutic interventions in preclinical studies. Collectively, this body of work addresses a number of outstanding questions about the validity of animal models of SCI and defines a biochemical outcome measure for animal studies with direct relevance to the clinical setting.

Our study employed a targeted proteomics approach to measure the abundance of 491 proteins in the CSF and serum. The definitive advantage of this approach is its ability to provide precise quantification in analytically challenging biofluids, with sensitivity comparable to that of antibody-based assays (57, 58). Moreover, unlike these assays, this approach can be readily applied to proteins for which reliable antibodies may not exist. Conversely, although our interrogation of several hundred proteins within the CSF and serum of human patients with SCI far exceeds any effort reported in the literature to date, our inferences are necessarily limited to the panel of proteins targeted here. An additional limitation of our study is the requirement that subjects complete a valid neurological examination within 24 h of admission; the possibility of important pathophysiological differences in patients unable to perform this examination cannot be excluded.

DATA AVAILABILITY

The raw mass spectrometry data have been deposited to the ProteomeXchange Consortium (59) *via* the MassIVE partner repository with the dataset identifier MSV000085567. Clinical and technical metadata and

processed protein abundance data are provided in supplemental Tables S3 and S4, respectively.

Supplemental Data—This article contains supplemental data.

Acknowledgments—This work was supported by Brain Canada, the Michael Smith Foundation for Health Research, Genome Canada, Genome BC, the Djavad Mowfaghian Center for Brain Health, the Praxis Spinal Cord Institute (formerly the Rick Hansen Institute), and the VGH & UBC Hospital Foundation. The authors are grateful for the expertise of the dedicated staff at the UBC Center for Comparative Medicine who helped to manage the health and welfare of the animals.

Funding and Additional Information—The analysis was enabled in part by the support provided by WestGrid and Compute Canada (to L. J. F.), and through computational resources and services provided by Advanced Research Computing at the University of British Columbia (to B. K. K. and L. J. F.). M. A. S. acknowledges support from the Canadian Institutes of Health Research (CIHR), a Vancouver Coastal Health–CIHR–UBC MD/PhD Studentship, and the Wings for Life Spinal Cord Research Foundation. Mass spectrometry infrastructure for L. J. F. and C. B. was supported by Genome BC and Genome Canada (214PRO). B. K. K. is the Canada Research Chair in Spinal Cord Injury and the Dvorak Chair in Spine Trauma.

Author Contributions—L. J. F. and B. K. K. conceptualization; M. A. S., C. S., and R. B. methodology; M. A. S. software; M. A. S., J. R., and A. M. J. validation; M. A. S. formal analysis; M. A. S., J. R., S. T., N. M., A. P., A. M. J., K. N., J. J., S. C., K. Shortt, Y. G.-K., K. So, A. F., R. G., E. B. O., M. A. R., K. D., and F. S. investigation; J. R., S. T., N. M., A. P., A. M. J., L. B., L. R., A. T., S. C., J.-M. M.-T., C. B., T. A., R. C.-M., N. D., J. R. W., S. D., S. P., J. S., C. G. F., and M. F. D. resources; J. R. and A. P. data curation; M. A. S., L. J. F., and B. K. K. writing-original draft; J. R., S. T., N. M., A. P., A. M. J., L. B., L. R., A. T., S. C., J.-M. M.-T., C. B., T. A., R. C.-M., N. D., J. R. W., S. D., S. P., J. S., C. G. F., M. F. D., M. A. S., K. N., J. J., S. C., K. Shortt, Y. G.-K., K. So, A. F., R. G., E. B. O., M. A. R., K. D., F. S., C. B., R. B., L. J. F., and B. K. K. writing-review and editing; M. A. S. visualization; C. B., L. J. F., and B. K. K. supervision; L. J. F. and B. K. K. project administration; B. K. K. funding acquisition.

Conflict of Interest—The authors declare no competing interests.

Abbreviations—The abbreviations used are: AIS, American Spinal Injury Association Impairment Scale; AUC, area under the receiver operating characteristic curve; CSF, cerebrospinal fluid; DE, differentially expressed; FA, formic acid; FDR, false discovery rate; GFAP, glial fibrillary acidic protein; GO, Gene Ontology; LLOQ, lower limit of quantitation; MRM, multiple reaction monitoring; NACC, neighborhood analysis of conserved coexpression; PCA, principal component analysis; PRM, parallel reaction monitoring; PTIBS, Porcine Thoracic Injury Behavioral Scale; SCI, spinal cord injury; SIS, stable isotope standard; TMS, total motor score.

Received February 6, 2021, and in revised from, April 14, 2021
Published, MCPRO Papers in Press, June 12, 2021, https://doi.org/10.1016/j.mcpro.2021.100096

REFERENCES

1. Singh, A., Tetreault, L., Kalsi-Ryan, S., Nouri, A., and Fehlings, M. G. (2014) Global prevalence and incidence of traumatic spinal cord injury. *Clin. Epidemiol.* **6**, 309–331
2. Priebe, M. M., Chiodo, A. E., Scelza, W. M., Kirshblum, S. C., Wuermser, L.-A., and Ho, C. H. (2007) Spinal cord injury medicine. 6. Economic and societal issues in spinal cord injury. *Arch. Phys. Med. Rehabil.* **88**, S84–S88
3. Krueger, H., Noonan, V. K., Trenaman, L. M., Joshi, P., and Rivers, C. S. (2013) The economic burden of traumatic spinal cord injury in Canada. *Chronic Dis. Inj. Can.* **33**, 113–122
4. Gomes-Osman, J., Cortes, M., Guest, J., and Pascual-Leone, A. (2016) A systematic review of experimental strategies aimed at improving motor function after acute and chronic spinal cord injury. *J. Neurotrauma* **33**, 425–438
5. Ramer, L. M., Ramer, M. S., and Bradbury, E. J. (2014) Restoring function after spinal cord injury: Towards clinical translation of experimental strategies. *Lancet Neurol.* **13**, 1241–1256
6. Ahuja, C. S., Wilson, J. R., Nori, S., Kotter, M. R. N., Druschel, C., Curt, A., and Fehlings, M. G. (2017) Traumatic spinal cord injury. *Nat. Rev. Dis. Primers* **3**, 17018
7. Tigchelaar, S., and Kwon, B. K. (2017). In: Weidner, N., Rupp, R., Tansey, K. E., eds. *Neurological Aspects of Spinal Cord Injury*, Springer International Publishing, Cham, Switzerland: 721–740
8. Lammertse, D. P. (2013) Clinical trials in spinal cord injury: Lessons learned on the path to translation. The 2011 International Spinal Cord Society Sir Ludwig Guttmann Lecture. *Spinal Cord* **51**, 2–9
9. Lee, R. S., Noonan, V. K., Batke, J., Ghag, A., Paquette, S. J., Boyd, M. C., Fisher, C. G., Street, J., Dvorak, M. F., and Kwon, B. K. (2012) Feasibility of patient recruitment into clinical trials of experimental treatments for acute spinal cord injury. *J. Clin. Neurosci.* **19**, 1338–1343
10. Fawcett, J. W., Curt, A., Steeves, J. D., Coleman, W. P., Tuszynski, M. H., Lammertse, D., Bartlett, P. F., Blight, A. R., Dietz, V., Ditunno, J., Dobkin, B. H., Havton, L. A., Ellaway, P. H., Fehlings, M. G., Privat, A., *et al*. (2007) Guidelines for the conduct of clinical trials for spinal cord injury as developed by the ICCP panel: Spontaneous recovery after spinal cord injury and statistical power needed for therapeutic clinical trials. *Spinal Cord* **45**, 190–205
11. Kwon, B. K., Bloom, O., Wanner, I.-B., Curt, A., Schwab, J. M., Fawcett, J., and Wang, K. K. (2019) Neurochemical biomarkers in spinal cord injury. *Spinal Cord* **57**, 819–831
12. Institute of Medicine (US) Forum on Neuroscience and Nervous System Disorders. (2013) *Improving the Utility and Translation of Animal Models for Nervous System Disorders: Workshop Summary*. National Academies Press (US), Washington DC
13. Sengupta, M. B., Basu, M., Iswarari, S., Mukhopadhyay, K. K., Sardar, K. P., Acharyya, B., Mohanty, P. K., and Mukhopadhyay, D. (2014) CSF proteomics of secondary phase spinal cord injury in human subjects: Perturbed molecular pathways post injury. *PLoS One* **9**, e110885
14. Moghieb, A., Bramlett, H. M., Das, J. H., Yang, Z., Selig, T., Yost, R. A., Wang, M. S., Dietrich, W. D., and Wang, K. K. W. (2016) Differential neuroproteomic and systems biology analysis of spinal cord injury. *Mol. Cell. Proteomics* **15**, 2379–2395
15. Kwon, B. K., Stammers, A. M. T., Belanger, L. M., Bernardo, A., Chan, D., Bishop, C. M., Slobogean, G. P., Zhang, H., Umedaly, H., Giffin, M., Street, J.,

Boyd, M. C., Paquette, S. J., Fisher, C. G., and Dvorak, M. F. (2010) Cerebrospinal fluid inflammatory cytokines and biomarkers of injury severity in acute human spinal cord injury. *J. Neurotrauma* **27**, 669–682
16. Streijger, F., Skinnider, M. A., Rogalski, J. C., Balshaw, R., Shannon, C. P., Prudova, A., Belanger, L., Ritchie, L., Tsang, A., Christie, S., Parent, S., Mac-Thiong, J.-M., Bailey, C., Urquhart, J., Ailon, T., *et al*. (2017) A targeted proteomics analysis of cerebrospinal fluid after acute human spinal cord injury. *J. Neurotrauma* **34**, 2054–2068
17. Hulme, C. H., Brown, S. J., Fuller, H. R., Riddell, J., Osman, A., Chowdhury, J., Kumar, N., Johnson, W. E., and Wright, K. T. (2017) The developing landscape of diagnostic and prognostic biomarkers for spinal cord injury in cerebrospinal fluid and blood. *Spinal Cord* **55**, 114–125
18. Ritchie, M. E., Phipson, B., Wu, D., Hu, Y., Law, C. W., Shi, W., and Smyth, G. K. (2015) Limma powers differential expression analyses for RNA-sequencing and microarray studies. *Nucleic Acids Res.* **43**, e47
19. Pedregosa, F., Varoquaux, G., Gramfort, A., Michel, V., Thirion, B., Grisel, O., Blondel, M., Prettenhofer, P., Weiss, R., Dubourg, V., Vanderplas, J., Passos, A., Cournapeau, D., Brucher, M., Perrot, M., *et al*. (2011) Scikit-learn: Machine learning in Python. *J. Machine Learn. Res.*, 2825–2830
20. Lee, J. H. T., Jones, C. F., Okon, E. B., Anderson, L., Tigchelaar, S., Kooner, P., Godbey, T., Chua, B., Gray, G., Hildebrandt, R., Cripton, P., Tetzlaff, W., and Kwon, B. K. (2013) A novel porcine model of traumatic thoracic spinal cord injury. *J. Neurotrauma* **30**, 142–159
21. Streijger, F., Lee, J. H. T., Chak, J., Dressler, D., Manouchehri, N., Okon, E. B., Anderson, L. M., Melnyk, A. D., Cripton, P. A., and Kwon, B. K. (2015) The effect of whole-body resonance vibration in a porcine model of spinal cord injury. *J. Neurotrauma* **32**, 908–921
22. Yue, F., Cheng, Y., Breschi, A., Vierstra, J., Wu, W., Ryba, T., Sandstrom, R., Ma, Z., Davis, C., Pope, B. D., Shen, Y., Pervouchine, D. D., Djebali, S., Thurman, R. E., Kaul, R., *et al*., Mouse ENCODE Consortium. (2014) A comparative encyclopedia of DNA elements in the mouse genome. *Nature* **515**, 355–364
23. Tigchelaar, S., Streijger, F., Sinha, S., Flibotte, S., Manouchehri, N., So, K., Shortt, K., Okon, E., Rizzuto, M. A., Malenica, I., Courtright-Lim, A., Eisen, A., Keuren-Jensen, K. V., Nislow, C., and Kwon, B. K. (2017) Serum micrornas reflect injury severity in a large animal model of thoracic spinal cord injury. *Sci. Rep.* **7**, 1376
24. Kuzyk, M. A., Smith, D., Yang, J., Cross, T. J., Jackson, A. M., Hardie, D. B., Anderson, N. L., and Borchers, C. H. (2009) Multiple reaction monitoring-based, multiplexed, absolute quantitation of 45 proteins in human plasma. *Mol. Cell. Proteomics* **8**, 1860–1877
25. Kuzyk, M. A., Parker, C. E., Domanski, D., and Borchers, C. H. (2013) Development of MRM-based assays for the absolute quantitation of plasma proteins. *Methods Mol. Biol.* **1023**, 53–82
26. Tyanova, S., Temu, T., and Cox, J. (2016) The MaxQuant computational platform for mass spectrometry-based shotgun proteomics. *Nat. Protoc.* **11**, 2301–2319
27. Mohammed, Y., Domański, D., Jackson, A. M., Smith, D. S., Deelder, A. M., Palmblad, M., and Borchers, C. H. (2014) PeptidePicker: A scientific workflow with web interface for selecting appropriate peptides for targeted proteomics experiments. *J. Proteomics* **106**, 151–161
28. Rogalski, J. C., Lin, M. S., Sniatynski, M. J., Taylor, R. J., Youhnovski, N., Przybylski, M., and Kast, J. (2005) Statistical evaluation of electrospray tandem mass spectra for optimized peptide fragmentation. *J. Am. Soc. Mass Spectrom.* **16**, 505–514
29. Pino, L. K., Searle, B. C., Bollinger, J. G., Nunn, B., MacLean, B., and MacCoss, M. J. (2020) The Skyline ecosystem: Informatics for quantitative mass spectrometry proteomics. *Mass Spectrom. Rev.* **39**, 229–244
30. Carr, S. A., Abbatiello, S. E., Ackermann, B. L., Borchers, C., Domon, B., Deutsch, E. W., Grant, R. P., Hoofnagle, A. N., Hüttenhain, R., Koomen, J. M., Liebler, D. C., Liu, T., MacLean, B., Mani, D. R., Mansfield, E., *et al*. (2014) Targeted peptide measurements in biology and medicine: Best practices for mass spectrometry-based assay development using a fit-for-purpose approach. *Mol. Cell. Proteomics* **13**, 907–917
31. Proc, J. L., Kuzyk, M. A., Hardie, D. B., Yang, J., Smith, D. S., Jackson, A. M., Parker, C. E., and Borchers, C. H. (2010) A quantitative study of the effects of chaotropic agents, surfactants, and solvents on the digestion efficiency of human plasma proteins by trypsin. *J. Proteome Res.* **9**, 5422–5437
32. Breschi, A., Djebali, S., Gillis, J., Pervouchine, D. D., Dobin, A., Davis, C. A., Gingeras, T. R., and Guigó, R. (2016) Gene-specific patterns of expression variation across organs and species. *Genome Biol.* **17**, 151
33. Csardi, G., and Nepusz, T. (2006) The igraph software package for complex network research. *InterJournal Complex Syst.* **1695**, 1–9
34. Monti, S., Tamayo, P., Mesirov, J., and Golub, T. (2003) Consensus clustering: A resampling-based method for class discovery and visualization of gene expression microarray data. *Mach. Learn.* **52**, 91–118
35. Alexa, A., Rahnenführer, J., and Lengauer, T. (2006) Improved scoring of functional groups from gene expression data by decorrelating GO graph structure. *Bioinformatics* **22**, 1600–1607
36. Falcon, S., and Gentleman, R. (2007) Using GOstats to test gene lists for GO term association. *Bioinformatics* **23**, 257–258
37. Olson, R. S., Cava, W. L., Mustahsan, Z., Varik, A., and Moore, J. H. (2018) Data-driven advice for applying machine learning to bioinformatics problems. *Pac. Symp. Biocomput.* **23**, 192–203
38. Zheng-Bradley, X., Rung, J., Parkinson, H., and Brazma, A. (2010) Large scale comparison of global gene expression patterns in human and mouse. *Genome Biol.* **11**, R124
39. Storey, J. D., and Tibshirani, R. (2003) Statistical significance for genome-wide studies. *Proc. Natl. Acad. Sci. U. S. A.* **100**, 9440–9445
40. Plaisier, S. B., Taschereau, R., Wong, J. A., and Graeber, T. G. (2010) Rank-rank hypergeometric overlap: Identification of statistically significant overlap between gene-expression signatures. *Nucleic Acids Res.* **38**, e169
41. Phipson, B., and Smyth, G. K. (2010) Permutation P-values should never be zero: Calculating exact P-values when permutations are randomly drawn. *Stat. Appl. Genet. Mol. Biol.* **9**. Article39
42. Giorgino, T. (2009) Computing and visualizing dynamic time warping alignments inR : Thedtw package. *J. Stat. Softw.* **31**
43. Schafer, S. T., Paquola, A. C. M., Stern, S., Gosselin, D., Ku, M., Pena, M., Kuret, T. J. M., Liyanage, M., Mansour, A. A., Jaeger, B. N., Marchetto, M. C., Glass, C. K., Mertens, J., and Gage, F. H. (2019) Pathological priming causes developmental gene network heterochronicity in autistic subject-derived neurons. *Nat. Neurosci.* **22**, 243–255
44. Bendixen, E., Danielsen, M., Larsen, K., and Bendixen, C. (2010) Advances in porcine genomics and proteomics–a toolbox for developing the pig as a model organism for molecular biomedical research. *Brief. Funct. Genomics* **9**, 208–219
45. Lubieniecka, J. M., Streijger, F., Lee, J. H. T., Stoynov, N., Liu, J., Mottus, R., Pfeifer, T., Kwon, B. K., Coorssen, J. R., Foster, L. J., Grigliatti, T. A., and Tetzlaff, W. (2011) Biomarkers for severity of spinal cord injury in the cerebrospinal fluid of rats. *PLoS One* **6**, e19247
46. Squair, J. W., Tigchelaar, S., Moon, K.-M., Liu, J., Tetzlaff, W., Kwon, B. K., Krassioukov, A. V., West, C. R., Foster, L. J., and Skinnider, M. A. (2018) Integrated systems analysis reveals conserved gene networks underlying response to spinal cord injury. *elife* **7**
47. van Middendorp, J. J., Hosman, A. J. F., and Doi, S. A. R. (2013) The effects of the timing of spinal surgery after traumatic spinal cord injury: A systematic review and meta-analysis. *J. Neurotrauma* **30**, 1781–1794
48. van Middendorp, J. J., Barbagallo, G., Schuetz, M., and Hosman, A. J. F. (2012) Design and rationale of a prospective, observational European multicenter study on the efficacy of acute surgical decompression after traumatic spinal cord injury: The SCI-POEM study. *Spinal Cord* **50**, 686–694
49. Geisler, F. H., Coleman, W. P., Grieco, G., Poonian, D., & Sygen Study Group. (2001) The Sygen multicenter acute spinal cord injury study. *Spine* **26**, S87–98
50. Fehlings, M. G., Vaccaro, A., Wilson, J. R., Singh, A., W Cadotte, D., Harrop, J. S., Aarabi, B., Shaffrey, C., Dvorak, M., Fisher, C., Arnold, P., Massicotte, E. M., Lewis, S., and Rampersaud, R. (2012) Early versus delayed decompression for traumatic cervical spinal cord injury: Results of the surgical timing in acute spinal cord injury study (STASCIS). *PLoS One* **7**, e32037
51. Pouw, M. H., Kwon, B. K., Verbeek, M. M., Vos, P. E., van Kampen, A., Fisher, C. G., Street, J., Paquette, S. J., Dvorak, M. F., Boyd, M. C., Hosman, A. J. F., and van de Meent, H. (2014) Structural biomarkers in the cerebrospinal fluid within 24 h after a traumatic spinal cord injury: A descriptive analysis of 16 subjects. *Spinal Cord* **52**, 428–433
52. Kwon, B. K., Streijger, F., Fallah, N., Noonan, V. K., Bélanger, L. M., Ritchie, L., Paquette, S. J., Ailon, T., Boyd, M. C., Street, J., Fisher, C. G., and Dvorak, M. F. (2017) Cerebrospinal fluid biomarkers to stratify injury severity and predict outcome in human traumatic spinal cord injury. *J. Neurotrauma* **34**, 567–580

53. Seok, J., Warren, H. S., Cuenca, A. G., Mindrinos, M. N., Baker, H. V., Xu, W., Richards, D. R., McDonald-Smith, G. P., Gao, H., Hennessy, L., Finnerty, C. C., López, C. M., Honari, S., Moore, E. E., Minei, J. P., *et al*. (2013) Genomic responses in mouse models poorly mimic human inflammatory diseases. *Proc. Natl. Acad. Sci. U. S. A.* **110**, 3507–3512
54. Takao, K., and Miyakawa, T. (2015) Genomic responses in mouse models greatly mimic human inflammatory diseases. *Proc. Natl. Acad. Sci. U. S. A.* **112**, 1167–1172
55. Normand, R., Du, W., Briller, M., Gaujoux, R., Starosvetsky, E., Ziv-Kenet, A., Shalev-Malul, G., Tibshirani, R. J., and Shen-Orr, S. S. (2018) Found in translation: A machine learning model for mouse-to-human inference. *Nat. Methods* **15**, 1067–1073
56. Courtine, G., Bunge, M. B., Fawcett, J. W., Grossman, R. G., Kaas, J. H., Lemon, R., Maier, I., Martin, J., Nudo, R. J., Ramon-Cueto, A., Rouiller, E. M., Schnell, L., Wannier, T., Schwab, M. E., and Edgerton, V. R. (2007) Can experiments in nonhuman primates expedite the translation of treatments for spinal cord injury in humans? *Nat. Med.* **13**, 561–566
57. Addona, T. A., Shi, X., Keshishian, H., Mani, D. R., Burgess, M., Gillette, M. A., Clauser, K. R., Shen, D., Lewis, G. D., Farrell, L. A., Fifer, M. A., Sabatine, M. S., Gerszten, R. E., and Carr, S. A. (2011) A pipeline that integrates the discovery and verification of plasma protein biomarkers reveals candidate markers for cardiovascular disease. *Nat. Biotechnol.* **29**, 635–643
58. Hüttenhain, R., Soste, M., Selevsek, N., Röst, H., Sethi, A., Carapito, C., Farrah, T., Deutsch, E. W., Kusebauch, U., Moritz, R. L., Niméus-Malmström, E., Rinner, O., and Aebersold, R. (2012) Reproducible quantification of cancer-associated proteins in body fluids using targeted proteomics. *Sci. Transl. Med.* **4**, 142ra94
59. Vizcaíno, J. A., Deutsch, E. W., Wang, R., Csordas, A., Reisinger, F., Ríos, D., Dianes, J. A., Sun, Z., Farrah, T., Bandeira, N., Binz, P.-A., Xenarios, I., Eisenacher, M., Mayer, G., Gatto, L., *et al*. (2014) ProteomeXchange provides globally coordinated proteomics data submission and dissemination. *Nat. Biotechnol.* **32**, 223–226